8.B.5
8.B.6

Nuclear Physics B18 (1970) 333–365. North-Holland Publishing Company

PHOTOPRODUCTION OF NEUTRAL RHO MESONS

H. ALVENSLEBEN, U. BECKER, William K. BERTRAM, M. CHEN, K. J. COHEN, T. M. KNASEL, R. MARSHALL, D. J. QUINN, M. ROHDE, G. H. SANDERS, H. SCHUBEL and Samuel C. C. TING

Deutsches Elektronen-Synchrotron (DESY), Hamburg, Germany
and
Department of Physics and Laboratory for Nuclear Science, Massachusetts Institute of Technology, Cambridge, Massachusetts 02139, USA

Received 26 January 1970

Abstract: We present results of measurements on photoproduction of ρ^0 mesons. Analysis of 10^5 measured π-pairs on protons in the energy region 2.6 – 6.8 GeV using various assumptions of rho production, indicates that $d\sigma/dt(t = 0)$ decreases with increasing energy similar to πN scattering. Analysis of 10^6 measured π-pairs from 13 complex nuclei in a four-dimensional data matrix $d\sigma/d\Omega dm(A, m, p, t_\perp)$ with dimensions 13, 20, 6 and 20, yields precise information on nuclear density distributions determined by ρ-production. We obtain for the Woods-Saxon radii $R(A) = (1.12 \pm 0.02)A^{\frac{1}{3}}$ fm, and using the vector-dominance model, $\sigma_{\rho N} = 26.7 \pm 2.0$ mb and $\gamma_\rho^2/4\pi = 0.57 \pm 0.10$.

1. INTRODUCTION

We present results on the photoproduction of neutral ρ mesons [1-4]

$$\gamma + A \rightarrow A + \rho^0 , \qquad \rho^0 \rightarrow \pi^+\pi^- , \tag{1}$$

from 14 elements: hydrogen ($A = 1$), beryllium (9), carbon (12), aluminium (27), titanium (47.9), copper (63.5), silver (107.9) cadmium (112.4), indium (114.7), tantalum (181), tungsten (183.9), gold (197), lead (207.2) and uranium (238.1).

The hydrogen data were measured at forward production angles with incident photon energies between 2.6 and 6.8 GeV and in the dipion mass (m) region from 500 to 1000 MeV/c^2. A total of 100 000 events were detected in order to measure the cross sections in energy intervals of $\Delta E_\gamma = 0.6$ GeV and in mass intervals of $\Delta m = 30$ MeV/c^2.

The purposes of the hydrogen measurement were:

(i) to study the detailed production mechanism of pion pairs from protons with no theoretical assumptions by accurately measuring the dipion spectrum as a function of both mass and energy,

(ii) to study the energy dependence of the forward ρ-production cross section by fitting the extensive data with various assumptions for the pro-

duction mechanism, mass, width, and a general polynomial background in all its dependent variables.

The complex nuclei measurements were made at forward angles and covered twenty intervals in the dipion mass region from 400 to 1000 MeV/c^2, six intervals in the dipion momentum (p) from 4.8 to 7.2 GeV/c, and twenty intervals in the transverse momentum transfer to the nucleus ($t_\perp$) from 0.0 to - 0.04 (GeV/c)^2. These measurements form a four-dimensional data matrix ($A, m, p, t_\perp$) = (13, 20, 6, 20) containing approximately one million measured π-pairs. The high statistics of this experiment (between 10^2 and 10^3 times more events than previous works) together with the large variety of elements used (twice that of previous experiments [3, 4]) enables us to make an accurate study of the following:

(i) The nuclear density distributions. For a given A, the t-dependence yields accurate information on the nuclear radius $R(A)$ seen by the ρ-meson.

(ii) The absolute and relative forward ρ-production cross sections $d\sigma/d\Omega dm(A, m, p, t_\perp)$. For fixed A, p and $t_\perp$, measurement of the dipion spectra as a function of mass alone provides a unique determination of the ρ line shape and the background and hence an accurate determination of the cross section.

(iii) The ρ-nucleon cross section $\sigma_{\rho N}$ and the $\gamma\rho$ coupling constant $\gamma_\rho^2/4\pi$.

Measurement of the nuclear-density distributions and the production cross sections from the thirteen elements determines the rate of reabsorption of ρ-mesons by nuclear matter and the effective forward production cross section per nucleon $|f_0|^2$. This yields $\sigma_{\rho N}$ and $\gamma_\rho^2/4\pi = \alpha\sigma_{\rho N}^2/64\pi\,|f_0|^2$ in a self-consistent manner. Since the original work of Lanzerotti et al. [1], several experiments have been done [3, 4] to investigate reaction (1) in order to determine $\sigma_{\rho N}$ and $\gamma_\rho^2/4\pi$. They have obtained different results and some of the results are different from the predictions of the vector-dominance model [5].

2. THE EXPERIMENT

The present experiment was carried out at the 7.5 GeV DESY electron synchrotron. A bremsstrahlung beam interacted in the target and the photoproduced pairs were detected by a large aperture magnetic spectrometer [6] shown in fig. 1a. For hydrogen the target length was 60 cm.

This spectrometer consists of dipole magnets (MD, MA, MB), scintillation counters ($L_1, L_2, L_3, L_4, R_1, R_2, R_3, R_4$), threshold Cerenkov counters (LC, RC, HL, HR), and scintillation-counter hodoscopes (TL, TR, QL, QR, VL, VR). The magnet MD (maximum field 18 kG over an effective volume $1.0\times1.5\times0.3$ m^3) separates charged particles from the γ-beam and also sweeps very low-energy particles out of the system. Particles with a central spectrometer momentum are bent an angle of $15^\circ - \theta_\pm$ by MD, where $\theta_\pm$ is the horizontally projected production angle with respect to the beam. To isolate the beam and associated low-energy particles from the aperture of the spectrometer, considerable shielding is placed within the field re-

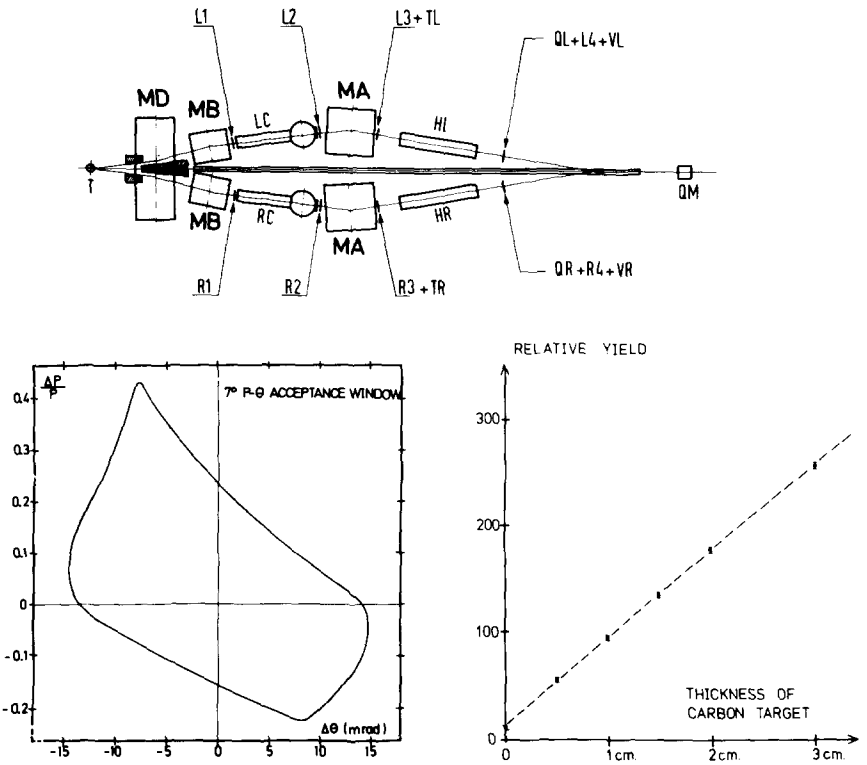

Fig. 1. (a) Plan view of the spectrometer. (b) Spectrometer acceptance limits. The locus of the limiting trajectories is shown as a function of $\Delta p/p_0$ and $\Delta\theta$ as defined in the text. The central spectrometer angle θ_0 is 7°. (c) The yield of pion pairs as a function of target thickness.

gion of MD. However, the shielding is in all cases at least 5 cm away from the limiting trajectories of accepted particles and thus is never a source of scattered background. After passing through MD, the central momentum particles are bent - 8° by the MB ($1.029\times0.30\times0.106$ m^3 effective field volume) located 2.18 m downstream from the centre of MD.

The target position and the field of MD are chosen such that the trajectory of the central ray (central momentum p_0 and angle θ_0) after it enters the MB magnets is identical for all settings of the spectrometer. The MA magnets, 5.39 m further downstream, then bend the central ray a constant angle - 12.93°. (The MA magnets have an effective field volume of $1.30\times 0.488\times0.166$ m^3). This arrangement has the following properties essential to the experiment:

(i) The acceptance of the spectrometer is not limited by the edges of magnets or by shielding, being defined instead by the scintillation trigger counters L_2 - L_4, R_2 - R_4. All counters are located such that their sur-

faces are not directly exposed to the target. The instantaneous rate in L_2 and R_2, the "hottest" of the triggering counters, is always $\lesssim 1.5$MHz; in all other counters it is always < 100 kHz.

(ii) The spread in position and angle of the particles as they pass through all the threshold counters is nearly independent of the spectrometer setting. Therefore, any slight inefficiency of these counters cannot lead to a momentum-transfer-dependent effect.

(iii) The spectrometer recombines rays of constant $p_\pm\theta_\pm \propto m$ and therefore has a large acceptance and at the same time a good mass resolution. For a given spectrometer setting, the acceptance is $\Delta p/p_0 \approx \pm 0.18$, $\Delta\theta/\theta_0 \approx \pm 0.14$, $\Delta m/m \approx \pm 0.10$, and $\Delta\psi \approx \pm 10$ mrad, where ψ is the projected vertical production angle. Fig. 1b shows a typical θp acceptance window for one of the spectrometer arms for $\theta_0 = 7^\circ$. The curve shows the limiting trajectories. Vacuum pipes and helium filled bags were placed inside the spectrometer to reduce multiple scattering and nuclear absorption of pions, so that the 22500 hodoscope combinations defined an event to an accuracy of $\delta m = \pm 15$ MeV/c^2, $\delta p = \pm 150$ MeV/c, and $\delta l_\perp = \pm 0.001$ (GeV/c)^2.

During the experiment many precautions were taken to ensure that the spectrometer behaved as designed and that all systematic effects were understood. We list the following 10 examples:

(i) To ensure that the data are not sensitive to second-order effects in the target, such as photon beam attenuation and pion absorption, we measured the yield of π-pairs as a function of target thickness from 0 to 5 g/cm^2 of carbon. As seen in fig. 1c, within an accuracy of 1%, the corrected counting rate increased linearly with target thickness.

(ii) Accidental coincidences were monitored by a series of duplicate logic circuits of different resolving times and were kept below 2% by controlling the beam intensity.

(iii) The dead time of the electronics was monitored by continuously recording the single rates in the counters. The beam intensity was adjusted such that the dead time was less than 2%.

(iv) Nuclear absorption of pions by material in the spectrometer was investigated by introducing additional material and by varying the gas pressure in the Cerenkov counters. The measured loss of pairs agreed with cal culations based on published data [7].

(v) To avoid any possible effects from spectrometer asymmetry, half the data was taken at each polarity of the spectrometer. The rates from the two spectrometer polarities were identical.

(vi) All counter voltages were kept constant to ± 5 V and all magnetic fields were kept stable to 3 parts in 10^4.

(vii) To ensure that low-mass π-pairs from high Z elements are not contaminated by electron pairs, Čerenkov counters were used to count and to reject electrons. They indicated the maximum contamination was less than 1 part in 10^4.

(viii) To ensure the reproducibility of the data, monitor runs were made on carbon every few hours at a fixed spectrometer setting of $\theta_0 = 5.5^\circ$, $p_0 = 3.35$ GeV/c. Over the entire running period the system was reproducible to ±1%.

(ix) To keep errors from inelastic contributions to reaction (1) small, all the data were taken with p close to the peak photon energy k_{max} ($k_{max}\ p \approx 1.2$).

(x) The purity of the targets was chosen to be better than 99.9%. The thickness of the targets was chosen such that the corrections for beam attenuation and for pion absorption were similar for each element and that the target-out rates were small.

3. THE DATA

The data were corrected for small systematic effects such as beam attenuation in the target, target out, nuclear absorption of pions in the target and in the counters, dead time, accidentals, etc. All of these corrections were checked by measurement in the same spectrometer to be accurate to 1%.

The acceptance was calculated by a Monte-Carlo method. A sufficient number of Monte-Carlo events was generated so that the errors in the measured cross sections are due only to experimental statistics and small systematic uncertainties. Essential to the Monte-Carlo integration was the accurate determination of the magnet-transport equations. Because of the accuracy needed, neither first-order nor second-order transport theory could be used. Instead, the equations were determined by numerically integrating a family of 100 trajectories through a grid of the measured field values of each magnet. The transport coefficients were then obtained from the trajectories by a least-squares method. The transport equations included all terms linear, bilinear, and pure quadratic in x, x', z, z' and $\Delta p/p_0$ (except those excluded by symmetry) and terms up to fourth order in $(\Delta p/p_0)/(1+\Delta p/p_0)$. Trajectories obtained from these coefficients agreed in position and angle to three parts in 10^3 with those obtained from exact numerical integration. The effects of multiple scattering and of π-decay in flight along the spectrometer were also considered in the Monte-Carlo calculation.

3.1. *Hydrogen data*

Table 1 shows the measured hydrogen cross sections at forward angles as a function of m from 505 - 955 MeV/c^2 and of p from 2.9 - 6.5 GeV/c. In obtaining these cross sections at forward production angles ($< 1^{\circ}$) the effects of the t variable ($|t_\perp| \approx 0.01$ (GeV/c)^2) and decay angular distribution have been folded into the acceptance [1]. We have used a t-dependence of $\exp(8t)$ and a decay angular distribution in the centre of mass of $\frac{3}{2}\sin^2\theta_{c.m.}$. Fig. 2a shows the hydrogen data in three dimensions with the measured experimental cross sections displayed as a function of the variables m and p. These data enable direct comparison to various models in a straightforward way. Two principal features appear in fig. 2a.

(i) The spectra are dominated by the ρ.

(ii) For every mass bin from 505 to 955 MeV/c^2, the spectrum exhibits a dependence of the type $d\sigma/d\Omega dm \propto p^2(1+M/p)^2$ with $M > 0$, rather than a

Table 1
Hydrogen data matrix $d\sigma/d\Omega dm$ in units of $\mu b/sr \cdot MeV/c^2$ as a function of p (GeV/c), the laboratory momentum of the dipions, and m (MeV/c^2), the invariant mass of the pion pair.

m \ p	6.5	5.9	5.3	4.7	4.1	3.5	2.9
955	.51 ± .13	.29 ± .06	.38 ± .12	.25 ± .11			
925	.57 ± .10	.42 ± .08	.55 ± .10	.52 ± .11	.17 ± .12		
895	1.06 ± .11	.59 ± .08	.64 ± .09	.60 ± .09	.53 ± .11	1.02 ± .48	
865	1.32 ± .14	1.24 ± .09	1.16 ± .10	.87 ± .09	.62 ± .09	.38 ± .09	.26 ± .13
835	2.55 ± .16	2.20 ± .11	2.11 ± .12	1.48 ± .09	1.39 ± .13	.92 ± .12	.49 ± .10
805	4.08 ± .19	3.62 ± .15	3.20 ± .14	2.63 ± .11	2.34 ± .14	1.43 ± .15	1.09 ± .20
775	6.86 ± .21	6.09 ± .17	5.23 ± .18	4.33 ± .13	3.67 ± .16	2.80 ± .19	1.70 ± .29
745	8.21 ± .25	7.42 ± .18	6.17 ± .20	5.07 ± .17	4.24 ± .16	3.42 ± .23	2.17 ± .20
715	7.26 ± .22	7.07 ± .17	6.08 ± .18	5.11 ± .19	4.54 ± .18	2.79 ± .19	2.14 ± .15
685	6.29 ± .23	5.85 ± .17	5.45 ± .17	3.96 ± .17	3.47 ± .20	2.73 ± .25	2.17 ± .22
655	5.23 ± .25	4.84 ± .15	4.59 ± .18	3.65 ± .16	3.19 ± .20	3.20 ± .51	1.13 ± .21
625	4.18 ± .32	4.50 ± .16	3.84 ± .17	2.68 ± .15	3.02 ± .19	1.08 ± .85	1.17 ± .14
595	3.13 ± .25	4.05 ± .23	3.49 ± .16	2.34 ± .14	2.23 ± .18	1.49 ± .38	.73 ± .33
565	3.44 ± .21	3.21 ± .22	3.56 ± .20	2.15 ± .13	1.67 ± .14	2.78 ± .69	.70 ± .18
535	2.82 ± .26	3.17 ± .15	3.24 ± .30	2.26 ± .15	2.12 ± .15	2.21 ± .44	.81 ± .09
505	5.17 ± .80	2.96 ± .17	2.77 ± .18	1.33 ± .28	2.07 ± .16	1.28 ± .34	.95 ± .17

p^2 dependence (fig. 2b). This behaviour shows that the forward dipion production cross section $d\sigma/dt/dm$ decreases with increasing energy, similar to the case of πN scattering [8].

3.2. *Complex nuclei data*

To facilitate analysis and to be able to study the dependence of these cross sections on all dynamic variables we have grouped the data into a four-dimensional data matrix $(A, m, p, t_\perp) = (13, 20, 6, 20)$. Due to space limitations, these 31200 cross sections cannot all be presented here; we present some of the data and the results of a complete analysis.

Table 2 shows a typical subset of data for $p = 5.8$, 6.2, 6.6 GeV/c and $t_\perp = 0.0$ to -0.01 (GeV/c)^2, $k_{max} = 7.4$ GeV, in the mass region of 480 - 1020 MeV/c^2 for the 13 elements.

A projection of 2% of the data onto the three-dimensional $(A, m, t_\perp)$ space for $p = 6.2 \pm 0.2$ GeV/c is shown in fig. 3a. One observes that these spectra are dominated by the ρ and that the ρ is diffractively produced off the nucleus. As seen, the mass profile varies drastically with A and $t_\perp$, indicating that not all pion pairs are from ρ-decay and that there must exist an appreciable non-resonant background which depends on A, m and $t_\perp$. A projection of 5% of the data onto the (A, m) plane for $\langle p \rangle = 6.0$ GeV/c is shown in fig. 3b. In obtaining this figure, the experimental cross section $d\sigma/d\Omega dm$ was divided by $p^2 (f_c + f_{inc})$ (see subsect. 4.3). We thus remove the ρ-production mechanism but not the background from the mass spectra.

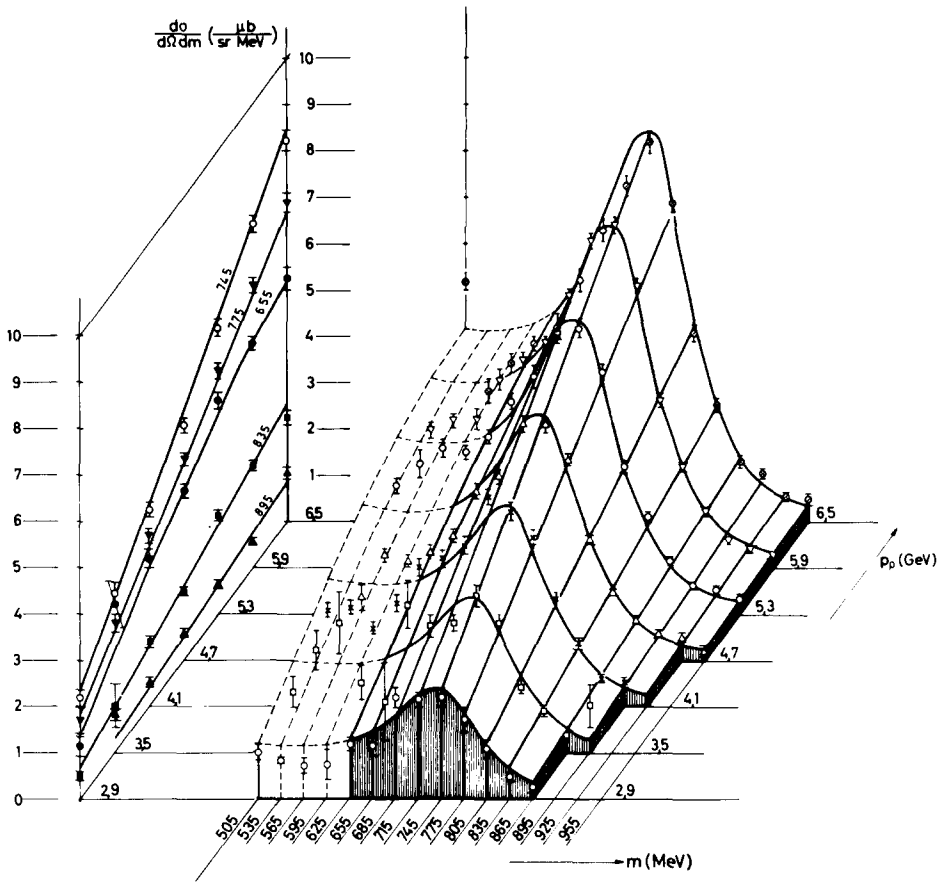

Fig. 2. (a) Experimentally measured cross sections $d\sigma/d\Omega dm$ in $\mu b/sr \cdot MeV/c^2$ of reaction (1) for hydrogen as a function of the variables m and p. The curves are best fits to eq. (2) (the background is not shown). Similar curves were obtained for fits to eqs. (3) and (4). (b) Projection of fig. 2a onto the $(p, d\sigma/d\Omega dm)$ plane for fixed values of m. The curves are best fits to $d\sigma/d\Omega dm = p^2(1 + M/p)^2$. This shows explicitly that the data for fixed m increase more slowly than p^2 $(M > 0)$.

In the absence of background, all spectra should be identical. As seen, the width and shape of the spectra (full width half maximum) varies considerably from low A to high A elements. This is further evidence that the non-resonant background depends strongly on A.

Table 2

TABLE 2

BERYLLIUM $\frac{1}{A}\frac{d^2\sigma}{d\Omega\, dm}$ in μb/sr.MeV/c^2 vs. m(MeV/c^2),p(GeV/c) and $t_\perp$ (GeV/c)^2

-T =	0.001	0.003	0.005	0.007	0.009
M			P = 5.8 GEV/C		
495	11.3 ± 2.2	5.7 ± 3.0	13.1 ± 4.2	6.1 ± 5.2	7.9 ± 4.9
525	11.0 ± 1.8	6.9 ± 2.6	9.5 ± 3.5	5.4 ± 2.5	4.9 ± 3.0
555	12.0 ± 1.7	11.5 ± 2.5	12.2 ± 3.2	14.6 ± 4.6	9.8 ± 3.9
585	12.9 ± 1.6	7.7 ± 2.2	11.1 ± 3.5	15.2 ± 4.7	13.5 ± 5.0
615	16.1 ± 1.3	14.4 ± 2.3	7.1 ± 2.3	5.6 ± 2.8	8.2 ± 3.9
645	17.0 ± 1.4	14.7 ± 2.1	13.0 ± 2.1	7.8 ± 3.5	13.6 ± 3.8
675	21.8 ± 1.5	17.9 ± 2.4	22.9 ± 3.3	11.7 ± 2.7	13.9 ± 4.6
705	30.6 ± 1.5	26.2 ± 2.3	23.4 ± 2.6	19.0 ± 3.1	20.1 ± 5.0
735	36.1 ± 1.5	29.7 ± 2.1	30.1 ± 2.9	29.9 ± 3.0	29.8 ± 3.5
765	32.1 ± 1.8	27.9 ± 2.6	20.9 ± 2.9	19.9 ± 3.3	20.1 ± 3.4
795	20.2 ± 1.8	15.9 ± 2.6	10.3 ± 2.7	16.7 ± 5.7	10.1 ± 8.2
825	12.1 ± 1.4	8.1 ± 2.1	7.1 ± 2.5	4.0 ± 2.1	9.9 ± 3.2
855	9.0 ± 1.3	6.7 ± 2.2	6.9 ± 2.0	4.9 ± 2.6	3.5 ± 2.3
885	5.2 ± 1.2	2.1 ± 1.3	2.8 ± 2.0	3.6 ± 2.6	-3.7 ± 5.3
915	1.7 ± 0.8	2.3 ± 1.3	4.8 ± 2.9	12.4 ± 5.6	
945	1.7 ± 0.8	2.3 ± 1.3	1.2 ± 1.3	1.2 ± 1.3	
975	0.5 ± 0.6				
1005	1.1 ± 1.1				
M			P = 6.2 GEV/C		
495	12.2 ± 4.9	14.5 ± 8.6	32.2 ± 51.6		
525	10.2 ± 2.3	9.7 ± 4.0	8.0 ± 3.8	10.8 ± 6.4	9.0 ± 4.3
555	13.0 ± 2.0	15.0 ± 3.3	17.0 ± 4.3	7.8 ± 3.3	5.3 ± 4.8
585	12.7 ± 1.9	16.2 ± 3.0	11.8 ± 3.7	10.0 ± 3.7	8.1 ± 3.0
615	15.9 ± 1.6	18.8 ± 2.8	14.3 ± 2.9	13.6 ± 3.7	18.8 ± 6.2
645	22.3 ± 1.4	15.8 ± 2.1	12.8 ± 2.5	8.3 ± 2.4	13.6 ± 3.3
675	23.2 ± 1.4	21.7 ± 2.3	22.6 ± 2.5	20.8 ± 3.5	14.6 ± 2.4
705	30.6 ± 1.7	28.5 ± 2.6	26.7 ± 3.6	22.7 ± 3.2	26.0 ± 5.9
735	38.6 ± 1.9	37.2 ± 2.6	25.7 ± 2.9	26.9 ± 3.3	33.7 ± 4.8
765	39.9 ± 1.8	41.1 ± 2.7	29.1 ± 3.0	29.9 ± 3.1	26.2 ± 2.8
795	25.8 ± 1.4	21.5 ± 2.0	20.8 ± 2.4	18.5 ± 2.8	17.7 ± 2.9
825	15.1 ± 1.4	9.2 ± 2.7	10.2 ± 2.3	11.2 ± 2.6	8.5 ± 3.0
855	9.0 ± 1.2	5.3 ± 1.6	6.7 ± 2.1	7.4 ± 2.9	7.8 ± 3.4
885	4.3 ± 0.9	2.8 ± 1.4	2.2 ± 1.4	4.0 ± 1.8	4.1 ± 2.0
915	2.9 ± 0.7	1.2 ± 0.9	2.7 ± 1.4	3.1 ± 1.6	-0.6 ± 1.1
945	0.7 ± 0.9	1.9 ± 1.2	2.7 ± 2.1	9.3 ± 5.5	
975	0.4 ± 1.0	0.9 ± 1.0	0.3 ± 2.4		
1005	1.0 ± 0.7	0.8 ± 0.8			
M			P = 6.6 GEV/C		
495					
525	32.5 ± 15.6		14.5 ± 13.2		
555	12.5 ± 3.3	9.1 ± 5.1	13.4 ± 5.0	12.2 ± 6.6	16.8 ± 7.0
585	14.5 ± 2.5	15.2 ± 4.0	12.9 ± 3.4	13.6 ± 4.3	0.2 ± 4.0
615	18.0 ± 2.6	14.9 ± 3.8	9.0 ± 3.3	13.0 ± 5.2	18.8 ± 5.3
645	24.5 ± 2.1	22.2 ± 3.1	15.4 ± 3.4	18.1 ± 3.4	15.8 ± 5.8
675	24.8 ± 1.7	21.7 ± 2.5	23.6 ± 3.2	14.5 ± 3.0	12.0 ± 2.7
705	32.4 ± 1.9	37.8 ± 3.2	30.0 ± 2.8	29.6 ± 4.1	22.4 ± 3.5
735	40.3 ± 2.2	39.0 ± 3.3	43.2 ± 4.2	26.2 ± 3.2	26.0 ± 5.2
765	43.9 ± 2.4	39.9 ± 3.0	35.9 ± 4.2	26.5 ± 3.5	29.1 ± 4.2
795	28.8 ± 1.7	24.3 ± 2.4	22.2 ± 2.5	20.5 ± 3.5	14.5 ± 2.5
825	14.8 ± 1.1	14.4 ± 1.9	11.3 ± 1.8	11.5 ± 2.1	9.7 ± 2.9
855	7.3 ± 1.1	7.9 ± 1.4	7.5 ± 2.2	2.7 ± 1.9	3.1 ± 1.6
885	4.7 ± 1.0	2.7 ± 1.1	1.6 ± 1.3	3.6 ± 2.0	0.6 ± 1.6
915	2.0 ± 0.8	1.0 ± 1.0	0.6 ± 0.7	3.3 ± 1.5	0.4 ± 1.4
945	2.2 ± 0.6	1.5 ± 0.8	-0.1 ± 0.9	1.3 ± 1.2	5.5 ± 4.1
975	1.3 ± 0.6		4.1 ± 3.4		
1005	3.1 ± 2.2	2.0 ± 2.0			1.7 ± 1.8

Table 2 (continued)

TABLE 2 CONTINUED

CARBON $\frac{1}{A}\frac{d^2\sigma}{d\Omega dm}$ in μb/sr.MeV/c^2 vs. m(MeV/c^2),p(GeV/c) and $t_\perp$ (GeV/c)^2

-T =	0.001	0.003	0.005	0.007	0.009
M			P = 5.8 GEV/C		
495	10.9 ± 1.8	5.2 ± 3.4	5.0 ± 2.6	6.2 ± 3.6	6.0 ± 3.8
525	14.9 ± 1.9	13.7 ± 3.2	11.4 ± 3.2	10.2 ± 3.5	4.9 ± 2.6
555	13.1 ± 2.1	10.8 ± 2.5	7.4 ± 2.9	11.1 ± 3.8	9.4 ± 4.5
585	17.1 ± 2.0	11.1 ± 2.6	13.4 ± 4.0	10.6 ± 5.1	12.0 ± 5.5
615	16.8 ± 1.5	13.1 ± 2.3	18.8 ± 3.8	11.3 ± 4.9	13.5 ± 5.0
645	22.2 ± 1.8	20.2 ± 2.5	14.2 ± 2.3	8.4 ± 5.2	12.5 ± 3.8
675	26.6 ± 1.7	25.3 ± 2.7	20.2 ± 3.2	12.0 ± 2.9	16.3 ± 5.0
705	31.1 ± 1.5	28.8 ± 2.4	27.0 ± 2.7	24.2 ± 3.3	16.4 ± 4.6
735	40.8 ± 1.6	31.3 ± 2.2	34.9 ± 3.1	31.5 ± 3.0	29.8 ± 3.4
765	39.8 ± 2.0	35.4 ± 2.9	34.7 ± 3.6	23.0 ± 3.5	20.9 ± 3.4
795	26.8 ± 2.0	23.8 ± 3.8	13.8 ± 3.8	17.9 ± 8.2	8.6 ± 9.1
825	16.2 ± 1.8	17.7 ± 3.0	18.9 ± 4.5	10.9 ± 4.1	10.7 ± 4.0
855	10.6 ± 1.6	4.0 ± 2.1	7.1 ± 2.3	10.5 ± 4.2	0.2 ± 1.8
885	6.6 ± 1.3	2.1 ± 1.3	0.3 ± 1.4	1.9 ± 1.9	-4.2 ± 5.9
915	3.3 ± 0.8	4.0 ± 1.2	1.9 ± 1.2	3.2 ± 1.9	3.1 ± 2.8
945	1.4 ± 0.6	1.2 ± 0.6	2.0 ± 1.1	2.9 ± 1.3	0.8 ± 0.9
975	0.3 ± 0.3	0.0 ± 0.8	2.2 ± 1.3	-0.4 ± 2.2	2.0 ± 1.6
1005	1.4 ± 0.8		1.0 ± 1.3		
M			P = 6.2 GEV/C		
495	14.4 ± 4.2	-3.8 ± 8.7	98.9 ± 79.6	5.4 ± 52.7	
525	12.2 ± 2.5	13.5 ± 3.9	11.5 ± 3.8	19.1 ± 7.4	9.5 ± 3.8
555	14.4 ± 2.0	14.2 ± 3.1	8.6 ± 3.2	13.4 ± 3.6	2.6 ± 4.8
585	18.4 ± 2.1	16.2 ± 3.6	17.3 ± 4.5	18.0 ± 5.2	7.2 ± 3.0
615	16.6 ± 1.9	18.8 ± 3.5	19.9 ± 3.6	19.2 ± 4.9	9.3 ± 4.5
645	22.9 ± 1.6	22.1 ± 2.7	14.2 ± 2.8	11.8 ± 3.2	15.8 ± 4.1
675	31.4 ± 1.7	25.8 ± 2.6	23.5 ± 2.7	18.1 ± 3.3	15.6 ± 2.6
705	37.5 ± 1.9	35.3 ± 2.9	33.5 ± 3.8	27.6 ± 3.5	34.5 ± 6.8
735	46.4 ± 2.1	46.6 ± 2.9	33.6 ± 3.1	34.3 ± 3.6	37.4 ± 4.9
765	46.6 ± 1.9	47.3 ± 2.9	37.8 ± 3.4	36.6 ± 3.3	29.5 ± 2.9
795	32.4 ± 1.6	21.5 ± 2.0	25.9 ± 2.7	15.3 ± 2.7	18.2 ± 2.9
825	17.6 ± 1.5	19.2 ± 3.7	4.5 ± 1.7	16.6 ± 3.5	15.4 ± 4.3
855	8.8 ± 1.4	9.0 ± 1.9	12.4 ± 3.2	13.5 ± 4.3	5.2 ± 2.5
885	5.6 ± 1.2	6.1 ± 2.0	1.3 ± 1.1	6.9 ± 3.0	4.2 ± 3.4
915	2.7 ± 0.7	3.9 ± 1.4	6.3 ± 3.9	5.1 ± 2.8	1.7 ± 2.1
945	2.9 ± 0.8	0.5 ± 0.8	1.5 ± 1.1	4.8 ± 2.4	5.5 ± 3.7
975	2.0 ± 0.8	1.9 ± 1.0	0.0 ± 1.1	1.5 ± 0.9	1.7 ± 1.0
1005	0.9 ± 0.4	0.0 ± 0.8	1.0 ± 0.8		
M			P = 6.6 GEV/C		
495					
525	16.5 ± 9.7	24.3 ± 16.1	32.9 ± 17.2	13.0 ± 17.9	
555	15.1 ± 3.2	23.0 ± 6.5	16.5 ± 5.1	23.8 ± 7.1	20.9 ± 6.7
585	22.5 ± 2.8	25.2 ± 5.0	6.1 ± 2.7	7.6 ± 3.3	17.8 ± 6.2
615	27.2 ± 3.0	13.7 ± 4.1	20.1 ± 5.1	4.6 ± 5.8	8.8 ± 5.3
645	25.3 ± 2.3	24.3 ± 3.5	18.6 ± 3.7	18.1 ± 3.8	11.5 ± 5.3
675	32.5 ± 2.0	32.7 ± 3.2	25.1 ± 3.5	24.8 ± 4.2	19.3 ± 4.2
705	47.5 ± 2.3	40.9 ± 3.4	33.9 ± 3.0	24.4 ± 3.7	22.8 ± 3.6
735	54.1 ± 2.5	44.4 ± 3.6	42.0 ± 4.1	39.3 ± 3.9	31.4 ± 5.4
765	46.1 ± 2.4	48.0 ± 3.2	40.4 ± 4.4	32.3 ± 3.8	32.9 ± 4.3
795	34.0 ± 1.8	31.1 ± 2.7	24.5 ± 2.7	25.5 ± 3.8	19.7 ± 2.8
825	17.6 ± 1.2	18.4 ± 2.1	17.8 ± 2.1	8.7 ± 1.8	8.8 ± 2.8
855	8.6 ± 1.2	11.8 ± 1.8	6.6 ± 2.5	7.2 ± 2.9	4.0 ± 1.7
885	6.0 ± 1.1	7.5 ± 1.9	1.2 ± 2.1	4.0 ± 3.6	4.9 ± 3.3
915	3.2 ± 0.9	5.9 ± 1.9	5.2 ± 2.0	4.5 ± 2.0	3.6 ± 2.2
945	4.2 ± 1.0	2.6 ± 1.2	3.2 ± 2.3	1.6 ± 1.6	6.0 ± 4.6
975	2.5 ± 0.8	2.3 ± 1.1	0.7 ± 1.4	2.7 ± 2.8	-1.5 ± 3.1
1005	1.3 ± 0.6	1.2 ± 0.9			1.3 ± 1.1

Table 2 (continued)

TABLE 2 CONTINUED

ALUMINIUM $\frac{1}{A}\frac{d^2\sigma}{d\Omega dm}$ in μb/sr.MeV/c^2 vs. m(MeV/c^2),p(GeV/c) and $t_\perp$ (GeV/c)^2

-t =	0.001	0.003	0.005	0.007	0.009
M			P = 5.8 GEV/C		
495	17.6 ± 3.8	12.8 ± 5.6	10.0 ± 5.4	10.6 ± 9.7	4.3 ± 4.8
525	15.6 ± 2.9	17.3 ± 5.0	11.2 ± 5.0	14.3 ± 5.3	14.4 ± 6.0
555	23.4 ± 3.2	20.8 ± 4.1	14.5 ± 4.5	6.9 ± 4.4	11.4 ± 5.9
585	23.8 ± 2.8	16.6 ± 4.2	18.3 ± 5.9	6.5 ± 4.9	2.0 ± 2.9
615	26.3 ± 2.3	12.9 ± 2.9	11.0 ± 3.7	7.8 ± 5.2	9.3 ± 5.3
645	30.8 ± 2.5	27.0 ± 3.8	16.7 ± 3.3	6.6 ± 5.3	20.6 ± 6.0
675	32.5 ± 2.5	34.8 ± 4.5	19.6 ± 4.1	27.1 ± 5.4	15.8 ± 6.9
705	51.4 ± 2.5	39.8 ± 3.7	28.2 ± 3.7	30.9 ± 4.9	23.5 ± 7.0
735	68.1 ± 2.6	49.4 ± 3.4	45.0 ± 4.5	41.5 ± 4.3	36.5 ± 4.7
765	61.7 ± 3.1	53.2 ± 4.5	45.7 ± 5.3	35.8 ± 5.4	31.4 ± 5.2
795	40.7 ± 3.2	27.3 ± 4.9	46.9 ± 6.8	32.0 ± 10.4	50.1 ± 26.0
825	24.3 ± 2.7	26.3 ± 5.1	15.8 ± 4.8	6.8 ± 3.8	20.4 ± 6.2
855	17.6 ± 2.5	18.6 ± 5.1	8.0 ± 3.0	16.4 ± 6.4	4.4 ± 3.3
885	7.3 ± 2.0	6.3 ± 2.9	1.6 ± 3.0	5.3 ± 5.1	0.5 ± 15.2
915	4.0 ± 1.6	3.7 ± 2.1	2.4 ± 2.7		
945	1.6 ± 0.9	2.4 ± 1.7	3.7 ± 2.8	3.5 ± 2.7	2.8 ± 3.2
975	1.6 ± 1.3	5.7 ± 4.1	2.6 ± 2.8	3.8 ± 4.2	3.6 ± 4.1
1005	3.4 ± 2.5	11.5 ± 12.2	1.6 ± 3.1		
M			P = 6.2 GEV/C		
495	14.3 ± 7.6	15.9 ± 11.4	56.3 ± 91.0	198.5 ±203.3	
525	14.5 ± 3.8	11.2 ± 6.5	12.3 ± 6.5	23.4 ± 11.7	11.3 ± 5.8
555	22.7 ± 3.5	21.5 ± 5.4	16.9 ± 5.6	5.1 ± 3.9	0.8 ± 6.9
585	23.7 ± 3.5	20.3 ± 4.4	15.3 ± 5.9	14.0 ± 6.1	7.2 ± 3.8
615	26.4 ± 2.8	27.4 ± 4.3	16.3 ± 4.3	14.7 ± 5.1	0.0 ± 2.9
645	37.3 ± 2.5	23.6 ± 3.6	24.7 ± 4.5	8.2 ± 3.9	9.2 ± 4.1
675	47.5 ± 2.7	41.1 ± 4.2	27.3 ± 3.6	30.4 ± 5.6	19.5 ± 3.9
705	65.4 ± 3.3	45.2 ± 4.3	50.5 ± 6.3	31.1 ± 5.0	25.2 ± 7.9
735	83.8 ± 3.6	61.5 ± 4.3	46.5 ± 4.9	46.8 ± 5.8	27.6 ± 6.0
765	73.0 ± 3.1	67.4 ± 4.3	51.8 ± 5.0	52.2 ± 4.8	37.6 ± 4.3
795	47.7 ± 2.4	31.7 ± 3.1	32.2 ± 3.7	19.8 ± 4.0	24.5 ± 4.1
825	30.0 ± 2.4	25.9 ± 6.0	12.5 ± 3.3	10.8 ± 3.4	20.7 ± 6.4
855	18.5 ± 2.4	8.9 ± 2.9	5.3 ± 2.6	6.8 ± 3.8	5.0 ± 5.1
885	9.7 ± 1.9	8.7 ± 3.5	3.7 ± 2.6	6.7 ± 3.2	3.7 ± 2.6
915	4.3 ± 1.3	1.4 ± 1.5	4.5 ± 2.5	3.6 ± 3.9	-0.2 ± 2.1
945	2.3 ± 1.9	2.8 ± 2.2	2.5 ± 2.5	11.7 ± 8.4	6.5 ± 7.5
975	4.4 ± 2.4	3.5 ± 2.3	-1.4 ± 2.8	1.8 ± 1.9	2.2 ± 2.6
1005	3.6 ± 1.5	4.6 ± 2.6			
M			P = 6.6 GEV/C		
495					
525	9.0 ± 10.6		11.8 ± 15.1		
555	40.6 ± 7.3	37.4 ± 12.4	6.4 ± 5.4	27.0 ± 11.2	9.7 ± 6.3
585	28.6 ± 4.7	17.3 ± 5.9	14.0 ± 4.8	11.2 ± 5.5	-0.7 ± 7.0
615	23.0 ± 4.3	24.1 ± 6.5	22.4 ± 6.9	14.4 ± 7.6	5.1 ± 4.8
645	38.0 ± 3.4	25.2 ± 4.4	30.2 ± 6.3	11.2 ± 3.9	14.3 ± 7.0
675	47.6 ± 3.1	39.3 ± 4.4	36.6 ± 5.1	16.8 ± 4.6	18.1 ± 4.7
705	65.6 ± 3.6	52.1 ± 5.1	52.0 ± 4.8	33.9 ± 5.7	35.3 ± 5.9
735	77.5 ± 4.0	61.4 ± 5.6	53.4 ± 6.2	47.4 ± 5.8	46.6 ± 9.1
765	78.5 ± 4.1	65.0 ± 5.0	55.7 ± 7.2	50.0 ± 6.2	36.5 ± 5.8
795	55.7 ± 3.0	40.8 ± 4.0	30.7 ± 3.9	27.1 ± 5.2	25.2 ± 4.3
825	33.2 ± 2.0	22.9 ± 2.9	17.4 ± 2.8	18.6 ± 3.3	14.5 ± 4.7
855	16.9 ± 2.0	17.5 ± 2.7	14.6 ± 3.9	8.1 ± 4.1	6.9 ± 3.5
885	10.1 ± 1.8	5.2 ± 2.2	2.9 ± 1.9	4.4 ± 3.1	1.9 ± 3.7
915	7.8 ± 1.9	7.4 ± 2.8	8.1 ± 2.9	6.0 ± 2.9	5.2 ± 3.5
945	2.9 ± 1.1	3.1 ± 1.6	0.5 ± 2.1	4.9 ± 3.1	4.5 ± 2.8
975	0.6 ± 0.7				3.7 ± 2.8
1005	1.1 ± 1.2				

Table 2 (continued)

TABLE 2 CONTINUED

TITANIUM $\frac{1}{A}\frac{d^2\sigma}{d\Omega dm}$ in μb/sr.MeV/c^2 vs. m(MeV/c^2),p(GeV/c) and t_1 (GeV/c)^2

-T =	0.001	0.003	0.005	0.007	0.009
M	P = 5.8 GEV/C				
495	23.5 ± 5.1	12.1 ± 7.3	5.4 ± 5.9	0.5 ± 10.4	11.4 ± 9.2
525	23.4 ± 4.0	17.4 ± 6.3	11.3 ± 5.8	0.1 ± 2.8	3.0 ± 3.0
555	32.9 ± 4.3	18.4 ± 4.4	6.1 ± 3.5	16.6 ± 6.9	8.0 ± 5.2
585	30.1 ± 3.8	20.4 ± 5.4	8.6 ± 5.4	9.4 ± 6.8	12.2 ± 6.5
615	32.2 ± 2.8	14.9 ± 5.4	20.2 ± 5.4	21.7 ± 7.5	-0.8 ± 2.0
645	43.7 ± 3.3	30.9 ± 4.7	26.2 ± 4.4	4.5 ± 6.5	15.7 ± 5.8
675	52.6 ± 3.6	32.2 ± 5.1	31.2 ± 5.8	11.3 ± 4.8	24.1 ± 9.4
705	55.6 ± 3.4	58.4 ± 5.6	39.9 ± 5.6	28.6 ± 6.2	18.0 ± 8.9
735	81.0 ± 3.8	62.4 ± 5.0	53.1 ± 6.6	47.4 ± 6.2	29.8 ± 6.0
765	86.2 ± 4.9	61.0 ± 6.4	59.5 ± 7.7	23.1 ± 6.4	14.8 ± 5.5
795	55.4 ± 4.7	36.0 ± 6.8	27.4 ± 6.9	56.8 ± 16.2	9.0 ± 13.6
825	35.2 ± 3.9	23.4 ± 6.1	25.6 ± 7.4	14.1 ± 6.5	11.4 ± 5.6
855	22.8 ± 3.4	13.0 ± 5.2	16.6 ± 4.8	13.9 ± 6.9	1.1 ± 3.2
885	8.8 ± 2.7	3.9 ± 3.0	0.0 ± 2.6	10.0 ± 11.1	-8.3 ± 11.8
915	4.4 ± 2.0	5.5 ± 3.3	5.2 ± 4.2	9.2 ± 8.2	
945	3.9 ± 1.8	1.8 ± 1.8		3.9 ± 3.9	1.7 ± 3.4
975	0.0 ± 1.2		1.7 ± 3.5	7.8 ± 6.8	
1005	1.3 ± 2.6	4.2 ± 8.3			
M	P = 6.2 GEV/C				
495	18.9 ± 10.5	21.4 ± 15.3			133.1 ±139.3
525	22.1 ± 5.5	19.0 ± 9.4	14.6 ± 8.9	3.9 ± 7.8	14.3 ± 7.2
555	23.8 ± 4.2	21.9 ± 6.8	20.7 ± 7.5	4.2 ± 4.4	3.9 ± 10.2
585	39.0 ± 5.1	37.0 ± 6.6	13.4 ± 6.7	2.4 ± 4.1	4.5 ± 3.9
615	33.0 ± 3.6	34.2 ± 5.4	27.4 ± 6.0	9.4 ± 4.1	9.8 ± 7.0
645	46.2 ± 3.1	38.9 ± 5.2	26.4 ± 5.3	11.4 ± 4.8	7.5 ± 6.0
675	58.1 ± 3.3	37.5 ± 4.6	30.1 ± 4.2	22.8 ± 5.3	20.5 ± 4.3
705	70.1 ± 4.0	53.5 ± 5.4	46.7 ± 6.7	37.7 ± 6.3	21.2 ± 8.1
735	97.3 ± 4.9	75.6 ± 6.0	58.0 ± 7.0	46.1 ± 7.1	43.2 ± 8.8
765	99.5 ± 4.6	75.4 ± 6.1	48.9 ± 6.4	55.2 ± 6.6	44.3 ± 6.0
795	63.7 ± 3.7	45.1 ± 4.8	36.2 ± 5.4	34.6 ± 6.5	21.5 ± 5.2
825	37.5 ± 3.5	17.9 ± 6.5	16.3 ± 4.6	17.2 ± 5.3	13.1 ± 6.0
855	23.1 ± 3.2	24.0 ± 5.1	9.9 ± 4.1	18.8 ± 7.2	12.2 ± 8.0
885	11.2 ± 2.5	3.9 ± 3.6	12.8 ± 4.9	8.3 ± 4.2	2.2 ± 3.1
915	8.4 ± 2.0	5.3 ± 2.7	4.5 ± 2.8	4.4 ± 3.0	1.2 ± 2.3
945	0.9 ± 1.9	2.4 ± 3.8	1.4 ± 2.8		20.5 ± 26.0
975	3.0 ± 2.9		0.1 ± 5.9	2.7 ± 2.7	
1005	2.7 ± 1.6	2.0 ± 2.0	2.9 ± 3.0	18.6 ± 17.5	2.3 ± 4.7
M	P = 6.6 GEV/C				
495					
525	48.8 ± 28.9				
555	31.9 ± 8.1	27.3 ± 14.1	23.9 ± 11.4	24.2 ± 12.5	5.3 ± 6.0
585	32.5 ± 6.0	33.6 ± 9.0	11.9 ± 5.6	24.5 ± 8.5	-3.6 ± 7.8
615	38.1 ± 6.0	30.8 ± 8.6	22.4 ± 7.8	12.0 ± 8.6	13.3 ± 7.5
645	47.4 ± 4.5	40.5 ± 6.3	16.1 ± 6.3	21.4 ± 5.6	28.0 ± 11.1
675	63.9 ± 4.0	46.0 ± 5.5	39.7 ± 5.9	19.9 ± 5.9	22.3 ± 5.5
705	94.2 ± 4.8	72.5 ± 6.7	51.1 ± 5.5	44.6 ± 7.2	36.7 ± 6.7
735	118.3 ± 5.5	79.0 ± 7.3	52.8 ± 7.0	46.3 ± 6.3	40.4 ± 9.2
765	112.7 ± 5.8	95.9 ± 7.1	61.4 ± 9.1	48.2 ± 7.9	35.4 ± 6.6
795	77.5 ± 4.5	58.0 ± 6.0	38.0 ± 5.3	27.8 ± 7.1	18.4 ± 5.3
825	45.3 ± 3.0	31.5 ± 4.4	19.8 ± 4.1	24.0 ± 4.7	11.8 ± 5.6
855	28.3 ± 3.3	24.7 ± 4.1	8.2 ± 4.4	13.8 ± 6.4	6.8 ± 4.0
885	14.8 ± 2.8	11.9 ± 3.6	11.5 ± 4.6	17.8 ± 7.4	1.9 ± 4.1
915	8.7 ± 2.5	7.3 ± 3.2	4.1 ± 2.7	4.9 ± 3.0	0.7 ± 3.3
945	5.8 ± 1.7	3.6 ± 2.1	4.2 ± 3.7	4.4 ± 6.2	7.5 ± 6.5
975	3.4 ± 1.6	6.5 ± 5.1	3.3 ± 4.6	5.2 ± 5.9	6.4 ± 7.0
1005	4.7 ± 2.6	2.5 ± 2.8	13.1 ± 8.1		

Table 2 (continued)

TABLE 2 CONTINUED

COPPER $\frac{1}{A}\frac{d^2\sigma}{d\Omega dm}$ in μb/sr.MeV/c^2 vs. m(MeV/c^2),p(GeV/c) and $t_\perp$ (GeV/c)^2

-T =	0.001	0.003	0.005	0.007	0.009
M			P = 5.8 GEV/C		
495	20.4 ± 4.2	14.8 ± 8.9	20.7 ± 8.0	4.9 ± 5.2	13.5 ± 9.8
525	19.3 ± 3.7	11.4 ± 6.1	13.0 ± 5.7	9.3 ± 6.6	2.4 ± 2.4
555	23.0 ± 4.9	17.0 ± 7.3	19.9 ± 7.6	17.1 ± 7.4	12.4 ± 8.1
585	27.1 ± 5.6	29.8 ± 6.4	16.7 ± 7.1	-1.0 ± 5.3	7.5 ± 5.9
615	34.8 ± 3.9	22.3 ± 4.4	22.3 ± 5.7	2.0 ± 6.3	12.4 ± 6.5
645	42.4 ± 4.0	34.4 ± 4.8	28.0 ± 4.5	14.0 ± 9.5	13.6 ± 5.1
675	57.2 ± 3.6	43.0 ± 5.4	34.8 ± 6.2	20.6 ± 5.3	33.8 ± 10.1
705	72.0 ± 3.5	54.6 ± 5.2	38.5 ± 5.2	20.7 ± 5.1	33.9 ± 9.9
735	95.4 ± 3.9	69.0 ± 4.9	59.5 ± 6.5	45.3 ± 5.6	20.0 ± 4.6
765	95.7 ± 4.7	54.7 ± 5.8	48.7 ± 6.8	22.1 ± 5.8	15.8 ± 5.0
795	68.7 ± 5.0	38.7 ± 7.7	39.6 ± 8.7	20.8 ± 14.9	22.8 ± 21.6
825	36.2 ± 4.1	32.4 ± 6.8	23.2 ± 7.5	30.0 ± 11.1	17.3 ± 8.5
855	29.6 ± 4.1	18.3 ± 6.2	11.9 ± 4.5	2.2 ± 5.1	6.2 ± 5.3
885	5.7 ± 2.5	16.9 ± 5.2	3.2 ± 3.8	7.7 ± 7.7	-7.7 ± 10.9
915	4.6 ± 2.4	5.8 ± 3.2	1.4 ± 2.9	3.2 ± 5.1	
945	5.6 ± 3.2	6.8 ± 3.4	5.2 ± 3.9	2.4 ± 2.6	
975	2.8 ± 1.7	0.3 ± 4.7		-2.1 ± 11.4	2.5 ± 5.0
1005	7.3 ± 4.3				
M			P = 6.2 GEV/C		
495	25.4 ± 9.1	-11.2 ± 24.2		-55.7 ± 111.3	
525	31.5 ± 6.7	36.4 ± 10.1	15.7 ± 7.8	16.5 ± 11.6	8.8 ± 5.3
555	28.4 ± 5.0	19.2 ± 6.5	17.6 ± 7.9	21.9 ± 7.2	1.0 ± 10.9
585	43.7 ± 5.2	24.6 ± 7.7	20.2 ± 8.5	7.4 ± 6.8	10.6 ± 6.0
615	28.3 ± 3.9	24.2 ± 6.1	37.2 ± 7.2	12.5 ± 6.1	-0.6 ± 3.7
645	52.8 ± 3.4	34.4 ± 4.8	18.4 ± 4.6	14.8 ± 5.3	17.8 ± 8.3
675	66.0 ± 3.4	41.9 ± 4.6	31.7 ± 4.4	24.7 ± 5.3	10.3 ± 3.1
705	90.1 ± 4.3	61.2 ± 5.6	45.9 ± 6.2	33.9 ± 5.4	20.6 ± 7.7
735	110.5 ± 4.9	84.7 ± 5.8	53.5 ± 6.1	38.9 ± 6.2	10.2 ± 5.1
765	110.5 ± 4.5	80.0 ± 5.8	55.8 ± 6.3	41.5 ± 5.5	26.4 ± 4.6
795	74.9 ± 3.9	47.7 ± 4.7	36.6 ± 5.1	31.8 ± 5.8	19.7 ± 4.6
825	45.2 ± 3.7	11.4 ± 5.0	6.6 ± 3.7	9.9 ± 3.6	11.0 ± 5.4
855	25.9 ± 3.6	16.5 ± 4.0	20.9 ± 6.7	0.0 ± 5.3	12.7 ± 6.1
885	13.9 ± 2.8	16.7 ± 4.8	4.5 ± 4.7	6.0 ± 4.2	-0.5 ± 1.5
915	8.7 ± 2.2	2.4 ± 2.3	2.8 ± 2.9	11.0 ± 7.2	1.4 ± 6.2
945	8.4 ± 2.7	7.3 ± 4.4	6.1 ± 4.9		8.4 ± 10.6
975	2.8 ± 2.0	2.1 ± 2.3			2.9 ± 3.5
1005	3.4 ± 1.8	-0.7 ± 3.8	2.7 ± 2.8		4.4 ± 4.5
M			P = 6.6 GEV/C		
495					
525	21.3 ± 17.8	41.7 ± 33.1	13.5 ± 17.3	55.5 ± 60.3	
555	15.2 ± 6.2	38.6 ± 14.1	10.2 ± 6.5	31.4 ± 13.3	13.7 ± 9.0
585	46.9 ± 6.6	31.1 ± 9.6	28.7 ± 8.3	17.2 ± 7.9	17.1 ± 8.8
615	42.4 ± 6.2	22.5 ± 9.8	17.7 ± 8.9	16.6 ± 15.3	-1.2 ± 9.7
645	57.3 ± 5.1	30.7 ± 6.1	21.2 ± 6.1	22.2 ± 6.4	16.4 ± 10.7
675	68.1 ± 4.1	46.0 ± 5.5	43.1 ± 6.3	29.9 ± 7.0	21.7 ± 8.4
705	96.4 ± 4.6	78.1 ± 6.5	47.5 ± 5.0	43.0 ± 6.6	30.6 ± 6.1
735	117.0 ± 5.1	83.9 ± 7.0	61.1 ± 6.9	42.2 ± 5.8	32.6 ± 7.6
765	116.7 ± 5.6	86.2 ± 6.4	50.1 ± 7.5	44.7 ± 6.9	46.5 ± 6.9
795	87.7 ± 4.4	62.6 ± 5.7	46.7 ± 5.5	27.5 ± 6.2	24.9 ± 5.3
825	43.4 ± 2.8	34.1 ± 4.3	30.3 ± 4.4	16.3 ± 3.8	4.4 ± 4.0
855	25.3 ± 3.1	21.8 ± 3.6	5.8 ± 4.6	2.8 ± 3.9	8.8 ± 3.9
885	17.7 ± 2.8	9.2 ± 3.4	6.0 ± 5.6	9.6 ± 7.0	2.6 ± 6.0
915	7.4 ± 2.1	6.1 ± 3.2	3.7 ± 2.9	1.2 ± 2.2	7.5 ± 4.9
945	6.8 ± 2.1	6.8 ± 3.0	-0.7 ± 1.4	6.1 ± 4.8	5.6 ± 4.1
975	4.5 ± 1.9	4.4 ± 2.7	11.2 ± 6.7	7.4 ± 6.0	-8.7 ± 17.3
1005	4.4 ± 4.5	3.9 ± 3.0		10.2 ± 12.0	

Table 2 (continued)

TABLE 2 CONTINUED

SILVER $\frac{1}{A}\frac{d^2\sigma}{dtdm}$ in μb/sr.MeV/c^2 vs. m(MeV/c^2),p(GeV/c) and $t_\perp$ (GeV/c)^2

-t =	0.001	0.003	0.005	0.007	0.009
M	P = 5.8 GEV/C				
495	24.2 ± 5.1	20.0 ± 7.8	9.3 ± 5.9	-1.2 ± 6.9	5.0 ± 6.2
525	30.7 ± 4.4	11.2 ± 5.2	3.9 ± 3.9	7.5 ± 4.1	2.2 ± 2.2
555	30.8 ± 4.2	22.2 ± 5.0	21.1 ± 5.8	4.2 ± 3.9	3.7 ± 3.6
585	43.3 ± 4.3	25.4 ± 5.7	8.5 ± 5.6	6.1 ± 5.2	4.6 ± 3.8
615	43.6 ± 3.1	28.6 ± 4.4	22.6 ± 5.5	5.4 ± 4.3	1.3 ± 3.4
645	48.8 ± 3.3	33.8 ± 4.1	18.0 ± 3.0	1.8 ± 4.2	10.6 ± 3.7
675	61.7 ± 3.3	43.4 ± 4.8	23.8 ± 4.0	16.4 ± 4.0	13.5 ± 5.2
705	82.5 ± 3.5	48.5 ± 4.6	33.3 ± 4.5	17.4 ± 4.1	17.1 ± 7.1
735	102.8 ± 3.9	65.9 ± 4.6	39.7 ± 5.3	30.0 ± 4.4	17.2 ± 4.0
765	100.1 ± 4.8	52.4 ± 5.5	34.4 ± 5.5	12.2 ± 4.6	10.6 ± 3.8
795	65.3 ± 4.6	42.3 ± 6.4	23.6 ± 5.8	26.1 ± 9.7	-3.3 ± 6.6
825	41.4 ± 3.8	24.9 ± 5.5	13.0 ± 4.4	16.5 ± 6.1	8.8 ± 3.7
855	23.2 ± 3.1	14.0 ± 4.5	6.6 ± 2.9	4.4 ± 3.8	1.2 ± 3.0
885	13.7 ± 3.0	4.1 ± 2.6	-0.7 ± 1.9	3.9 ± 5.5	-5.4 ± 7.6
915	7.5 ± 2.4	0.8 ± 1.5	5.9 ± 4.7	6.8 ± 13.6	
945	10.6 ± 2.8	1.5 ± 1.6	2.3 ± 2.4		
975	2.7 ± 1.9	2.5 ± 3.2	3.0 ± 3.2		3.2 ± 3.5
1005	2.3 ± 2.3				
M	P = 6.2 GEV/C				
495	24.2 ± 11.1				
525	46.9 ± 7.5	25.7 ± 10.4	20.2 ± 9.2	10.6 ± 10.3	5.4 ± 4.4
555	31.6 ± 4.7	19.5 ± 6.1	10.5 ± 5.0	4.6 ± 3.7	0.9 ± 7.2
585	31.9 ± 4.7	27.2 ± 5.6	13.0 ± 6.2	9.8 ± 5.6	9.4 ± 4.0
615	50.9 ± 4.3	33.7 ± 5.5	23.7 ± 5.4	13.1 ± 4.9	11.5 ± 7.6
645	56.1 ± 3.3	33.2 ± 4.4	22.0 ± 4.7	5.7 ± 3.3	9.7 ± 3.8
675	77.0 ± 3.4	43.0 ± 4.2	28.0 ± 3.7	20.4 ± 4.3	8.1 ± 2.2
705	101.3 ± 4.0	58.8 ± 4.8	40.2 ± 5.2	21.5 ± 4.0	13.9 ± 5.6
735	128.4 ± 5.2	84.4 ± 5.5	54.6 ± 5.8	29.4 ± 4.7	15.4 ± 4.6
765	113.3 ± 4.5	81.5 ± 5.7	50.5 ± 6.0	24.6 ± 4.0	17.8 ± 3.5
795	88.9 ± 4.5	44.7 ± 4.3	32.3 ± 4.5	13.8 ± 4.1	14.1 ± 3.6
825	56.4 ± 3.9	33.1 ± 7.6	10.6 ± 3.5	13.9 ± 4.1	2.5 ± 2.8
855	31.6 ± 3.4	20.2 ± 4.4	8.9 ± 3.4	4.4 ± 3.2	1.3 ± 4.2
885	16.1 ± 2.7	7.2 ± 3.7	7.9 ± 3.4	4.8 ± 2.7	-0.5 ± 1.1
915	9.8 ± 2.0	3.6 ± 2.3	6.9 ± 3.2	3.5 ± 2.7	-0.1 ± 1.7
945	4.3 ± 2.8	4.0 ± 2.7	3.9 ± 3.3	5.9 ± 6.1	
975	6.7 ± 3.5		-1.5 ± 3.0	2.0 ± 2.1	
1005	5.6 ± 2.2				3.3 ± 3.5
M	P = 6.6 GEV/C				
495					
525	86.3 ± 38.4	71.9 ± 45.7		54.8 ± 65.6	
555	43.9 ± 8.9	28.6 ± 13.3	6.4 ± 6.5	3.1 ± 6.1	
585	37.6 ± 6.2	37.6 ± 9.5	18.7 ± 6.3	11.2 ± 5.7	-0.4 ± 6.1
615	53.2 ± 6.6	19.9 ± 7.2	25.3 ± 8.3	15.1 ± 8.3	3.8 ± 4.3
645	64.3 ± 5.1	49.7 ± 7.0	26.5 ± 7.0	25.5 ± 6.1	6.4 ± 5.4
675	83.7 ± 4.3	57.4 ± 5.6	29.6 ± 5.0	19.8 ± 5.3	11.1 ± 3.8
705	110.0 ± 4.5	73.8 ± 5.9	45.4 ± 4.5	26.5 ± 4.9	15.0 ± 3.9
735	140.5 ± 5.2	84.3 ± 6.3	51.4 ± 5.6	35.8 ± 4.4	11.3 ± 4.1
765	135.3 ± 5.5	88.0 ± 5.9	51.3 ± 7.1	30.8 ± 5.3	15.0 ± 3.6
795	95.5 ± 4.4	69.8 ± 5.8	28.1 ± 4.2	16.1 ± 4.8	14.2 ± 3.9
825	58.1 ± 3.2	35.1 ± 4.5	16.2 ± 3.3	14.7 ± 3.2	6.8 ± 3.6
855	30.2 ± 3.2	20.0 ± 3.4	12.4 ± 4.4	3.9 ± 3.4	3.0 ± 2.9
885	16.2 ± 2.7	13.5 ± 3.5	8.1 ± 3.4	4.6 ± 3.7	1.2 ± 2.6
915	10.0 ± 2.4	8.0 ± 3.1	3.6 ± 2.1	2.0 ± 1.6	4.3 ± 3.1
945	6.6 ± 1.7	3.3 ± 1.6	0.7 ± 2.5	3.0 ± 2.8	1.7 ± 1.9
975	6.1 ± 2.1	3.1 ± 2.1	3.5 ± 4.7	5.0 ± 6.3	
1005	7.5 ± 3.8	5.8 ± 5.0	8.9 ± 7.2		

Table 2 (continued)

TABLE 2 CONTINUED

CADMIUM $\frac{1}{A}\frac{d^2\sigma}{d\Omega dm}$ in μb/sr.MeV/c^2 vs. m(MeV/c^2),p(GeV/c) and $t_\perp$ (GeV/c)^2

-T =	0.001	0.003	0.005	0.007	0.009
M			P = 5.8 GEV/C		
495	24.7 ± 6.5	9.0 ± 8.6	9.9 ± 8.6	-0.5 ± 12.2	6.3 ± 7.8
525	32.2 ± 5.5	14.0 ± 7.9	12.2 ± 7.3	6.4 ± 4.9	5.3 ± 3.9
555	34.0 ± 5.2	32.7 ± 6.4	13.7 ± 5.5	11.9 ± 7.0	4.2 ± 4.1
585	37.5 ± 4.6	21.7 ± 6.3	6.7 ± 5.1	10.0 ± 7.6	7.4 ± 4.5
615	45.9 ± 3.5	21.4 ± 4.5	12.5 ± 5.0	21.5 ± 7.7	2.7 ± 4.2
645	49.2 ± 3.5	32.6 ± 4.7	19.4 ± 3.6	3.4 ± 6.2	9.1 ± 3.8
675	65.9 ± 4.0	31.4 ± 5.0	26.4 ± 4.8	13.7 ± 4.6	7.7 ± 5.2
705	81.7 ± 4.3	42.5 ± 5.7	24.3 ± 5.4	17.3 ± 6.1	12.6 ± 8.1
735	106.8 ± 4.9	61.5 ± 5.7	42.2 ± 6.6	22.7 ± 4.9	17.0 ± 5.1
765	98.9 ± 5.9	56.7 ± 7.0	35.1 ± 7.2	12.3 ± 6.1	5.9 ± 4.3
795	71.9 ± 5.8	37.0 ± 7.0	28.2 ± 7.2	16.1 ± 8.5	16.8 ± 16.0
825	40.6 ± 4.7	29.2 ± 7.0	11.8 ± 4.4	18.8 ± 6.9	11.2 ± 4.7
855	24.8 ± 3.8	12.6 ± 5.0	14.6 ± 4.3	3.5 ± 3.9	5.5 ± 4.2
885	14.8 ± 3.9	11.2 ± 4.0	6.7 ± 4.9	4.4 ± 6.2	10.8 ± 24.0
915	10.3 ± 3.7	5.6 ± 3.7	4.7 ± 5.3		6.4 ± 6.9
945	3.3 ± 2.0	2.4 ± 2.5	14.8 ± 7.5	3.0 ± 3.4	
975	-0.6 ± 1.3	4.0 ± 5.1	4.7 ± 5.0		
1005	3.6 ± 3.7				
M			P = 6.2 GEV/C		
495	32.5 ± 15.7	26.6 ± 19.2			
525	22.4 ± 6.9	17.1 ± 11.7	19.5 ± 12.0	30.9 ± 18.5	16.8 ± 8.7
555	33.7 ± 5.9	20.2 ± 8.0	12.0 ± 7.1	15.6 ± 7.2	-5.2 ± 9.2
585	35.5 ± 6.2	25.8 ± 6.5	12.4 ± 7.9	15.4 ± 7.9	12.0 ± 5.2
615	44.5 ± 4.9	32.6 ± 6.1	23.5 ± 6.1	14.3 ± 5.7	17.7 ± 9.8
645	63.5 ± 3.8	28.9 ± 5.1	21.7 ± 5.3	6.8 ± 4.7	3.6 ± 3.0
675	67.9 ± 3.5	40.8 ± 4.7	35.2 ± 4.5	19.1 ± 4.9	13.5 ± 3.1
705	104.1 ± 4.6	66.3 ± 5.9	41.6 ± 6.1	14.6 ± 4.5	15.2 ± 6.5
735	131.3 ± 6.3	79.3 ± 6.3	46.9 ± 6.9	27.6 ± 5.9	22.4 ± 6.5
765	125.4 ± 5.6	82.8 ± 7.1	47.9 ± 7.2	29.4 ± 5.6	15.0 ± 4.3
795	86.6 ± 4.9	46.7 ± 5.5	32.6 ± 5.8	12.8 ± 5.4	8.7 ± 3.9
825	49.3 ± 4.2	22.8 ± 9.3	20.0 ± 5.5	16.3 ± 4.5	7.0 ± 4.1
855	24.0 ± 3.8	13.3 ± 5.3	13.4 ± 4.4	6.9 ± 4.5	2.5 ± 7.2
885	14.1 ± 3.1	0.4 ± 3.1	5.2 ± 4.0	4.2 ± 2.6	4.5 ± 2.8
915	10.4 ± 2.3	3.3 ± 2.6	4.6 ± 2.9	7.1 ± 4.6	0.4 ± 2.5
945	4.1 ± 4.4	2.2 ± 3.3			7.8 ± 9.4
975	2.0 ± 3.7	3.0 ± 3.3	-0.0 ± 7.6	3.2 ± 3.2	
1005	2.5 ± 1.9	5.5 ± 4.0			
M			P = 6.6 GEV/C		
495					
525	47.0 ± 32.1		18.8 ± 24.4		
555	34.8 ± 10.4	2.0 ± 14.4	16.2 ± 10.8	18.4 ± 13.5	12.3 ± 10.2
585	46.2 ± 8.3	45.2 ± 11.7	18.8 ± 7.5	14.4 ± 7.9	3.2 ± 10.7
615	67.3 ± 8.7	18.2 ± 9.4	17.7 ± 8.0	2.5 ± 9.1	8.3 ± 6.5
645	61.2 ± 6.0	38.8 ± 7.1	18.7 ± 8.0	6.5 ± 4.2	4.4 ± 6.0
675	85.5 ± 4.9	48.4 ± 6.1	34.4 ± 6.0	18.7 ± 6.4	5.9 ± 3.5
705	117.0 ± 5.3	74.1 ± 6.5	46.3 ± 5.3	27.8 ± 5.9	15.7 ± 4.8
735	147.0 ± 5.9	99.4 ± 7.7	59.3 ± 6.6	43.8 ± 5.5	16.6 ± 5.4
765	153.6 ± 6.6	79.9 ± 6.9	45.8 ± 8.2	27.2 ± 6.6	23.9 ± 5.1
795	101.2 ± 5.4	59.2 ± 6.3	36.7 ± 5.7	5.1 ± 5.7	11.7 ± 4.8
825	55.3 ± 3.7	31.5 ± 4.9	22.0 ± 4.7	7.9 ± 3.7	9.1 ± 4.9
855	30.7 ± 3.9	24.2 ± 4.3	14.6 ± 5.7	8.3 ± 5.6	4.9 ± 4.4
885	21.4 ± 3.7	19.0 ± 4.6	6.6 ± 3.8	5.1 ± 3.6	4.3 ± 4.2
915	12.0 ± 3.3	16.4 ± 4.5	5.4 ± 3.0	1.4 ± 2.3	1.7 ± 2.3
945	6.2 ± 1.9	5.0 ± 2.4	1.0 ± 3.2	11.4 ± 11.5	
975	5.4 ± 2.2	8.3 ± 5.0			3.5 ± 3.9
1005		4.5 ± 4.7		13.5 ± 16.0	

Table 2 (continued)

TABLE 2 CONTINUED

INDIUM $\frac{1}{A}\frac{d^2\sigma}{d\Omega dm}$ in μb/sr.MeV/c^2 vs. m(MeV/c^2),p(GeV/c) and $t_\perp$ (GeV/c)^2

-T =	0.001	0.003	0.005	0.007	0.009
M			P = 5.8 GEV/C		
495	31.7 ± 6.2	3.9 ± 6.0	0.3 ± 5.0	-2.0 ± 8.4	
525	28.0 ± 4.7	11.5 ± 6.2	7.6 ± 5.2	15.7 ± 6.0	2.3 ± 2.4
555	34.2 ± 4.7	26.8 ± 5.7	9.5 ± 4.3	3.8 ± 4.3	9.3 ± 5.7
585	40.7 ± 4.4	16.5 ± 5.3	8.4 ± 5.4	7.0 ± 6.0	6.9 ± 4.5
615	43.6 ± 3.3	26.6 ± 4.6	5.4 ± 3.4	12.8 ± 5.5	-0.8 ± 1.6
645	51.7 ± 3.6	27.9 ± 4.5	11.9 ± 3.1	9.3 ± 6.0	7.2 ± 3.5
675	57.7 ± 3.8	42.7 ± 5.7	23.1 ± 4.4	17.0 ± 4.9	4.1 ± 4.1
705	81.4 ± 4.0	48.9 ± 5.4	23.2 ± 4.7	16.0 ± 4.9	10.8 ± 6.9
735	103.3 ± 4.5	59.5 ± 5.1	43.2 ± 6.2	23.4 ± 4.5	14.8 ± 4.4
765	104.2 ± 5.5	61.3 ± 6.7	46.7 ± 7.2	13.6 ± 5.5	14.8 ± 4.6
795	71.4 ± 5.4	36.2 ± 6.4	28.7 ± 7.1	16.4 ± 8.2	2.5 ± 10.3
825	37.6 ± 4.0	33.1 ± 6.3	12.6 ± 4.5	14.3 ± 5.6	5.8 ± 3.5
855	19.2 ± 3.1	12.3 ± 4.6	10.7 ± 3.7	3.5 ± 4.4	7.6 ± 5.1
885	11.0 ± 3.1	11.5 ± 4.1	2.3 ± 3.4	8.4 ± 8.4	-6.9 ± 9.8
915	8.9 ± 3.0	4.9 ± 3.1	10.6 ± 6.4	5.6 ± 8.0	5.4 ± 5.6
945	4.4 ± 2.0	1.9 ± 1.9			
975	5.5 ± 2.9	3.2 ± 4.0			
1005					
M			P = 6.2 GEV/C		
495	22.4 ± 12.3	23.9 ± 17.3	107.0 ± 176.4		
525	29.9 ± 6.8	4.3 ± 7.2	12.1 ± 9.0		5.9 ± 4.9
555	30.0 ± 5.1	27.3 ± 7.6	19.8 ± 7.7	5.9 ± 4.7	0.1 ± 8.6
585	44.8 ± 5.7	41.0 ± 7.4	10.3 ± 6.4	1.9 ± 3.1	9.9 ± 4.3
615	44.8 ± 4.3	36.3 ± 5.8	20.7 ± 5.3	21.3 ± 6.7	4.3 ± 4.7
645	60.6 ± 3.7	29.4 ± 4.8	20.8 ± 4.9	5.5 ± 4.0	3.9 ± 2.6
675	74.2 ± 3.8	46.8 ± 5.0	30.8 ± 4.3	17.8 ± 4.6	10.6 ± 2.8
705	94.5 ± 4.5	65.2 ± 5.8	44.5 ± 6.4	27.2 ± 5.3	7.2 ± 4.5
735	132.6 ± 5.6	76.6 ± 6.1	52.5 ± 6.9	32.2 ± 5.9	14.9 ± 5.7
765	133.3 ± 5.4	90.2 ± 6.8	42.2 ± 6.5	29.0 ± 4.9	7.1 ± 3.1
795	83.0 ± 4.5	44.4 ± 5.0	37.1 ± 5.5	14.5 ± 4.8	7.2 ± 3.3
825	54.8 ± 4.2	19.6 ± 7.3	15.5 ± 4.5	13.7 ± 4.2	9.0 ± 4.4
855	27.7 ± 3.5	19.3 ± 4.9	13.8 ± 4.5	4.4 ± 3.2	4.4 ± 5.6
885	11.5 ± 2.5	2.2 ± 3.3	1.2 ± 1.6	0.4 ± 1.3	5.4 ± 2.9
915	14.5 ± 2.5	8.3 ± 3.1	8.0 ± 4.8	7.5 ± 6.1	1.5 ± 3.0
945	2.5 ± 3.3	1.4 ± 2.6		5.2 ± 6.5	
975	1.7 ± 2.8	2.4 ± 2.6	-2.0 ± 4.0		2.8 ± 3.4
1005	2.0 ± 1.5	2.2 ± 2.2		3.2 ± 6.3	1.9 ± 3.8
M			P = 6.6 GEV/C		
495					
525	98.7 ± 44.1	27.4 ± 30.2	84.6 ± 49.0		
555	44.5 ± 10.0	33.2 ± 15.9	30.6 ± 13.2	9.5 ± 8.5	14.2 ± 11.2
585	48.7 ± 7.5	49.2 ± 11.3	29.0 ± 8.0	0.1 ± 3.6	8.6 ± 8.8
615	57.1 ± 7.4	52.7 ± 10.7	21.8 ± 8.2	11.8 ± 8.6	6.0 ± 5.1
645	69.2 ± 5.7	44.9 ± 6.9	18.1 ± 6.6	20.9 ± 5.7	11.6 ± 7.5
675	83.8 ± 4.8	42.6 ± 5.5	31.8 ± 5.4	14.4 ± 5.6	13.8 ± 4.1
705	113.9 ± 5.3	84.3 ± 7.2	38.3 ± 4.8	25.4 ± 5.5	13.6 ± 4.3
735	145.7 ± 6.1	94.6 ± 7.7	57.7 ± 6.9	32.4 ± 5.0	15.6 ± 5.6
765	151.1 ± 6.6	89.8 ± 6.9	41.7 ± 7.8	22.8 ± 5.9	21.8 ± 5.0
795	96.9 ± 5.2	75.7 ± 6.8	27.5 ± 4.6	12.1 ± 5.6	9.9 ± 3.8
825	59.2 ± 3.6	37.7 ± 4.9	20.1 ± 4.1	10.1 ± 3.3	9.7 ± 4.3
855	30.9 ± 3.6	18.2 ± 3.5	6.7 ± 4.1	3.2 ± 3.7	2.6 ± 3.7
885	16.9 ± 3.1	8.7 ± 3.2	3.9 ± 2.9	5.5 ± 3.7	0.6 ± 2.0
915	11.7 ± 2.8	6.2 ± 3.2	9.9 ± 3.6	3.6 ± 2.3	0.9 ± 1.8
945	6.3 ± 1.7	5.2 ± 2.4	1.2 ± 3.2	4.1 ± 3.0	
975	5.9 ± 2.2	7.2 ± 4.3	4.3 ± 4.3	3.2 ± 6.4	
1005	8.7 ± 6.3	6.4 ± 3.9	5.8 ± 6.4		

Table 2 (continued)

TABLE 2 CONTINUED

TANTALUM $\frac{1}{A}\frac{d^2\sigma}{d\Omega dm}$ in μb/sr.MeV/c^2 vs. m(MeV/c^2),p(GeV/c) and $t_\perp$ (GeV/c)^2

-T =	0.001	0.003	0.005	0.007	0.009
M		P = 5.8 GEV/C			
495	20.7 ± 5.5	11.4 ± 7.4	9.0 ± 6.6	-4.0 ± 5.7	7.7 ± 7.6
525	27.5 ± 4.7	11.1 ± 6.4	6.5 ± 4.9	4.1 ± 3.2	2.4 ± 1.9
555	30.9 ± 4.6	26.4 ± 5.4	14.0 ± 5.0	4.1 ± 3.8	3.4 ± 2.7
585	39.6 ± 4.5	19.1 ± 5.8	7.5 ± 6.3	5.3 ± 4.9	2.6 ± 2.2
615	43.8 ± 3.4	20.2 ± 4.2	13.6 ± 4.4	1.5 ± 1.9	2.1 ± 2.8
645	54.3 ± 3.9	23.7 ± 4.1	10.3 ± 2.6	2.2 ± 4.4	1.1 ± 1.5
675	59.3 ± 3.8	20.1 ± 4.3	21.9 ± 4.0	9.1 ± 3.4	0.5 ± 2.4
705	83.0 ± 4.0	40.0 ± 4.7	12.1 ± 3.6	11.6 ± 3.8	4.9 ± 4.8
735	105.2 ± 4.2	53.3 ± 4.5	31.6 ± 4.7	16.1 ± 2.9	10.1 ± 2.7
765	97.0 ± 5.0	55.4 ± 5.8	26.0 ± 5.2	10.3 ± 4.3	4.0 ± 2.2
795	69.0 ± 5.0	27.8 ± 5.6	19.8 ± 5.1	23.4 ± 8.8	-3.3 ± 6.6
825	41.1 ± 3.7	25.1 ± 5.5	12.7 ± 4.1	7.3 ± 3.2	4.6 ± 2.2
855	20.7 ± 2.9	9.1 ± 3.8	8.6 ± 2.8	4.9 ± 3.8	2.6 ± 2.3
885	12.6 ± 3.0	5.1 ± 2.6	0.3 ± 2.3		-3.4 ± 9.5
915	6.6 ± 2.3	5.7 ± 3.2			
945	6.6 ± 2.8	4.2 ± 2.9			
975	-0.5 ± 1.1				
1005	9.6 ± 5.8				
M		P = 6.2 GEV/C			
495	16.4 ± 11.6	44.5 ± 23.1			
525	32.6 ± 7.0	0.9 ± 7.2	10.8 ± 8.4	6.2 ± 6.8	3.4 ± 3.2
555	38.8 ± 5.7	17.7 ± 6.8	15.0 ± 6.4	8.0 ± 4.3	-2.7 ± 4.9
585	37.6 ± 5.7	28.6 ± 6.2	9.0 ± 6.0	8.4 ± 4.9	2.1 ± 2.0
615	43.5 ± 4.4	30.5 ± 5.4	16.0 ± 4.8	14.5 ± 5.0	-0.5 ± 1.6
645	60.5 ± 3.7	25.1 ± 4.7	14.5 ± 4.3	-0.3 ± 2.6	4.2 ± 2.0
675	75.2 ± 3.8	45.5 ± 4.8	26.5 ± 3.9	7.8 ± 3.3	3.1 ± 1.4
705	106.4 ± 4.7	52.8 ± 5.2	29.1 ± 5.2	14.4 ± 3.7	4.8 ± 3.5
735	129.1 ± 5.4	62.3 ± 5.3	36.1 ± 5.5	10.6 ± 3.8	3.9 ± 3.1
765	122.5 ± 4.9	57.0 ± 5.3	34.4 ± 5.4	12.5 ± 3.1	6.8 ± 2.3
795	85.6 ± 5.9	41.1 ± 4.4	22.8 ± 4.0	7.7 ± 3.4	4.7 ± 1.9
825	51.3 ± 3.7	17.1 ± 7.6	5.0 ± 3.0	6.8 ± 2.4	5.1 ± 2.7
855	32.5 ± 3.4	14.9 ± 4.1	12.7 ± 3.6	5.4 ± 3.0	0.3 ± 3.7
885	16.1 ± 2.5	7.3 ± 3.6	4.6 ± 2.7	1.5 ± 1.4	1.7 ± 1.4
915	8.5 ± 1.7	5.5 ± 2.4	3.8 ± 1.9	6.9 ± 3.8	0.6 ± 3.1
945	7.0 ± 3.4	2.7 ± 2.2		2.2 ± 2.7	
975	8.5 ± 4.7	10.4 ± 5.7	0.1 ± 5.6		
1005	1.1 ± 1.2	4.8 ± 3.4	6.2 ± 4.5		
M		P = 6.6 GEV/C			
495					
525	81.8 ± 39.6				
555	31.4 ± 9.0	33.0 ± 16.0	1.6 ± 6.2	13.8 ± 10.4	
585	53.0 ± 7.8	36.2 ± 9.5	16.7 ± 6.1	16.5 ± 6.6	-2.6 ± 3.0
615	56.4 ± 7.6	33.9 ± 9.4	21.1 ± 8.0	5.0 ± 6.7	-0.1 ± 2.0
645	72.9 ± 5.9	41.2 ± 6.6	18.2 ± 6.6	7.5 ± 3.7	1.2 ± 2.7
675	90.1 ± 5.0	48.4 ± 6.0	20.5 ± 4.3	3.5 ± 3.9	3.6 ± 2.0
705	118.6 ± 5.5	57.6 ± 6.2	24.7 ± 4.1	14.5 ± 4.0	5.1 ± 2.3
735	159.7 ± 6.4	75.3 ± 6.9	54.9 ± 6.7	16.0 ± 3.6	1.0 ± 2.5
765	149.8 ± 6.5	80.7 ± 6.5	39.4 ± 7.4	11.8 ± 4.2	9.9 ± 2.6
795	106.1 ± 5.1	60.4 ± 5.8	21.7 ± 3.9	9.8 ± 4.2	1.7 ± 1.8
825	64.8 ± 3.5	28.3 ± 3.9	13.3 ± 3.2	6.3 ± 2.3	-0.2 ± 1.5
855	29.5 ± 3.3	21.2 ± 3.4	4.4 ± 3.2	2.9 ± 2.7	0.4 ± 1.1
885	21.4 ± 3.0	9.1 ± 2.8	4.3 ± 2.6	6.9 ± 2.8	1.1 ± 2.0
915	12.1 ± 2.5	6.2 ± 2.5	3.6 ± 1.9	0.4 ± 0.9	0.8 ± 1.3
945	7.8 ± 1.7	6.1 ± 2.1	0.4 ± 2.0		1.6 ± 2.3
975	6.0 ± 1.9	2.8 ± 3.0	2.7 ± 2.9		
1005	4.1 ± 3.5	3.9 ± 4.0		52.1 ± 94.2	

Table 2 (continued)

TABLE 2 CONTINUED

TUNGSTEN $\frac{1}{A}\frac{d^2\sigma}{d\Omega dm}$ in $\mu b/sr.MeV/c^2$ vs. $m(MeV/c^2)$, $p(GeV/c)$ and $t_\perp$ $(GeV/c)^2$

-T =	0.001	0.003	0.005	0.007	0.009
M			P = 5.8 GEV/C		
495	30.5 ± 8.4	11.3 ± 10.7	-0.6 ± 7.4	-1.0 ± 12.1	11.0 ± 10.8
525	30.3 ± 6.5	5.0 ± 8.7	12.0 ± 7.8	5.5 ± 4.6	5.1 ± 3.2
555	25.6 ± 5.7	21.9 ± 5.6	6.7 ± 4.5	8.1 ± 5.9	2.6 ± 2.7
585	35.8 ± 5.2	22.7 ± 7.7	1.2 ± 7.5	0.4 ± 6.2	2.3 ± 2.1
615	48.4 ± 3.9	21.1 ± 5.2	3.8 ± 3.8	9.4 ± 5.3	2.2 ± 3.0
645	57.7 ± 4.7	35.5 ± 5.7	11.5 ± 3.4	1.1 ± 5.9	3.1 ± 2.5
675	66.9 ± 4.8	37.4 ± 6.4	27.0 ± 5.1	6.7 ± 4.2	5.0 ± 4.2
705	88.7 ± 5.0	43.8 ± 6.4	29.8 ± 6.2	8.1 ± 5.0	3.1 ± 5.5
735	105.7 ± 5.2	56.7 ± 5.7	29.5 ± 5.8	24.5 ± 4.7	8.7 ± 3.4
765	101.3 ± 6.1	47.2 ± 7.2	29.0 ± 7.1	3.3 ± 5.5	8.3 ± 3.8
795	74.9 ± 6.5	31.8 ± 7.6	18.4 ± 6.6	22.9 ± 9.7	0.9 ± 13.4
825	38.6 ± 6.4	26.3 ± 9.5	22.8 ± 6.9	9.3 ± 5.3	7.5 ± 4.2
855	27.3 ± 5.7	21.0 ± 7.3	16.1 ± 5.9	4.1 ± 3.7	2.7 ± 2.8
885	10.1 ± 6.3	8.7 ± 4.6	-1.3 ± 2.6	6.1 ± 6.8	
915	5.9 ± 3.5	1.6 ± 3.1	6.0 ± 6.6	4.8 ± 9.6	9.2 ± 7.7
945	1.6 ± 1.6	3.3 ± 3.3	4.7 ± 4.9		4.8 ± 5.2
975	4.0 ± 3.7				
1005			8.0 ± 9.5		
M			P = 6.2 GEV/C		
495	10.1 ± 15.5	32.4 ± 23.9		279.2 ± 242.7	
525	44.8 ± 10.4	5.2 ± 11.8	0.9 ± 10.9	26.6 ± 16.8	
555	27.7 ± 6.8	10.9 ± 8.7	10.9 ± 7.7	11.7 ± 6.1	-3.3 ± 8.6
585	42.1 ± 7.8	32.7 ± 7.6	16.2 ± 9.4	8.3 ± 6.4	7.2 ± 3.2
615	42.4 ± 5.6	36.0 ± 6.8	17.4 ± 5.4	14.6 ± 5.4	-0.3 ± 2.6
645	62.2 ± 4.4	18.7 ± 5.4	10.3 ± 5.0	2.0 ± 4.0	2.9 ± 1.9
675	79.3 ± 4.5	42.7 ± 5.6	23.8 ± 4.3	13.1 ± 4.6	5.3 ± 2.0
705	102.3 ± 5.4	49.5 ± 6.2	13.7 ± 5.2	8.6 ± 4.1	6.1 ± 4.6
735	130.6 ± 6.4	71.8 ± 6.9	29.4 ± 6.9	17.3 ± 5.4	-0.5 ± 4.0
765	128.7 ± 6.0	68.6 ± 7.1	30.8 ± 6.6	16.1 ± 4.5	8.4 ± 3.3
795	89.6 ± 5.2	42.2 ± 5.6	18.1 ± 5.0	12.6 ± 5.2	2.0 ± 2.3
825	57.9 ± 4.7	24.0 ± 10.6	17.6 ± 5.5	7.0 ± 2.5	8.7 ± 3.9
855	23.3 ± 5.7	9.0 ± 7.4	9.8 ± 4.1	7.7 ± 4.8	-0.4 ± 5.7
885	12.5 ± 5.1	3.6 ± 13.7	2.0 ± 2.8	5.8 ± 3.2	
915	12.0 ± 3.3	2.2 ± 2.3	9.9 ± 6.4	2.4 ± 2.7	
945	-3.9 ± 7.8	-1.6 ± 3.2			4.6 ± 9.2
975	0.1 ± 4.3		0.1 ± 8.9	3.4 ± 3.5	
1005	1.8 ± 1.8		9.7 ± 7.0		6.0 ± 6.0
M			P = 6.6 GEV/C		
495					
525	19.8 ± 23.3	37.9 ± 40.8			
555	37.6 ± 13.0	9.6 ± 19.4	10.0 ± 10.7		11.0 ± 9.9
585	47.7 ± 10.2	32.0 ± 11.1	12.2 ± 7.6	11.0 ± 7.1	-3.6 ± 4.1
615	63.3 ± 10.1	53.6 ± 13.8	15.8 ± 8.1	10.5 ± 10.3	2.1 ± 3.6
645	69.1 ± 7.1	35.1 ± 7.5	24.9 ± 9.8	6.3 ± 4.4	9.9 ± 6.6
675	80.6 ± 5.7	35.0 ± 6.6	16.7 ± 5.1	6.0 ± 5.9	4.7 ± 2.7
705	109.3 ± 6.2	62.1 ± 7.2	30.3 ± 5.3	12.1 ± 4.5	2.3 ± 2.7
735	143.0 ± 7.0	80.7 ± 8.3	44.5 ± 6.8	14.3 ± 4.5	-0.9 ± 3.4
765	154.8 ± 7.7	84.6 ± 8.2	39.1 ± 9.4	1.2 ± 5.5	14.2 ± 3.4
795	106.7 ± 6.1	64.5 ± 7.0	29.0 ± 5.4	8.1 ± 5.8	3.9 ± 3.2
825	52.6 ± 3.8	32.7 ± 5.1	5.9 ± 4.0	3.1 ± 2.9	2.9 ± 2.9
855	31.6 ± 4.4	18.2 ± 3.6	1.8 ± 3.8	1.6 ± 4.1	1.4 ± 2.3
885	22.0 ± 5.1	10.1 ± 5.1	4.3 ± 3.5		0.8 ± 1.7
915	6.5 ± 6.3	10.0 ± 5.2	2.7 ± 2.9	3.2 ± 2.6	1.2 ± 2.3
945	9.0 ± 2.7	1.4 ± 1.6	0.1 ± 6.0		1.6 ± 1.9
975	10.5 ± 5.0	8.2 ± 6.3			
1005	8.9 ± 5.5				

Table 2 (continued)

TABLE 2 CONTINUED

GOLD $\frac{1}{A}\frac{d^2\sigma}{d\Omega dm}$ in μb/sr.MeV/c^2 vs. m(MeV/c^2),p(GeV/c) and $t_\perp$ (GeV/c)^2

-T =	0.001	0.003	0.005	0.007	0.009
M			P = 5.8 GEV/C		
495	21.8 ± 7.5	7.7 ± 9.9	4.2 ± 7.7	-5.7 ± 8.0	4.9 ± 6.9
525	22.7 ± 5.8	20.2 ± 9.7	7.5 ± 6.8	3.4 ± 3.8	3.5 ± 2.3
555	37.3 ± 6.0	24.6 ± 6.1	7.3 ± 4.6	4.8 ± 4.7	6.3 ± 3.9
585	40.0 ± 5.2	22.7 ± 7.6	0.3 ± 5.4	8.7 ± 6.7	1.9 ± 1.7
615	38.0 ± 3.4	10.9 ± 4.4	13.1 ± 5.1	10.3 ± 4.9	1.8 ± 2.9
645	54.9 ± 4.3	26.2 ± 4.6	11.3 ± 3.1	-0.7 ± 4.3	2.7 ± 1.9
675	64.8 ± 4.3	31.9 ± 5.4	24.5 ± 4.4	6.5 ± 3.5	3.2 ± 3.0
705	89.3 ± 4.9	30.3 ± 6.0	15.3 ± 5.2	2.6 ± 4.2	8.9 ± 6.6
735	102.6 ± 5.3	47.8 ± 5.7	25.1 ± 5.9	15.9 ± 4.1	7.5 ± 3.2
765	105.1 ± 6.6	47.3 ± 7.3	26.5 ± 6.9	5.2 ± 5.2	8.0 ± 3.7
795	67.9 ± 6.5	32.5 ± 7.4	29.8 ± 7.6	13.8 ± 7.1	0.3 ± 6.8
825	39.6 ± 6.4	32.3 ± 9.3	23.9 ± 6.8	8.0 ± 3.9	2.3 ± 2.0
855	25.9 ± 5.3	26.5 ± 7.6	12.6 ± 5.1	3.7 ± 3.3	
885	11.6 ± 6.1	16.0 ± 5.4	-1.1 ± 2.2		
915	15.7 ± 5.0	2.8 ± 3.0			
945	9.4 ± 4.0	6.3 ± 4.5			4.9 ± 5.3
975	0.1 ± 2.4	5.4 ± 6.8			
1005					
M			P = 6.2 GEV/C		
495	35.4 ± 19.1	32.0 ± 23.7			
525	35.5 ± 9.6	30.3 ± 16.2	-2.4 ± 8.8	8.3 ± 9.2	2.0 ± 2.8
555	34.0 ± 6.8	27.3 ± 10.0	13.1 ± 7.8	6.7 ± 4.8	-2.6 ± 7.2
585	37.1 ± 7.2	26.6 ± 6.9	20.4 ± 8.9	4.9 ± 5.0	4.3 ± 2.4
615	46.6 ± 5.5	29.3 ± 6.2	18.6 ± 5.5	12.6 ± 4.9	0.5 ± 2.4
645	64.6 ± 4.2	20.8 ± 5.1	11.0 ± 4.3	-1.9 ± 2.8	1.8 ± 1.4
675	88.1 ± 4.2	40.9 ± 5.0	22.2 ± 4.0	12.1 ± 3.8	1.9 ± 1.3
705	103.3 ± 4.9	46.3 ± 5.6	23.1 ± 5.1	5.0 ± 3.3	10.4 ± 4.2
735	134.9 ± 6.6	78.1 ± 6.7	32.6 ± 6.3	15.4 ± 4.5	3.1 ± 3.1
765	132.4 ± 6.1	74.4 ± 7.3	30.2 ± 6.6	17.7 ± 4.5	3.3 ± 2.6
795	92.3 ± 5.5	31.3 ± 5.3	18.0 ± 4.8	8.1 ± 4.7	3.0 ± 2.2
825	50.9 ± 4.7	19.2 ± 10.0	6.8 ± 4.3	6.6 ± 2.8	2.4 ± 2.0
855	26.1 ± 5.5	6.9 ± 7.4	11.5 ± 4.3	3.8 ± 3.0	0.2 ± 5.0
885	12.6 ± 4.9	10.6 ± 13.4	6.5 ± 6.8	5.9 ± 3.1	1.9 ± 2.4
915	15.6 ± 3.7	4.2 ± 3.1		2.2 ± 2.5	
945	-2.1 ± 7.7	3.2 ± 5.2		19.6 ± 15.2	
975	0.1 ± 4.1	4.0 ± 4.4	-2.8 ± 5.5		
1005	5.3 ± 3.1	3.7 ± 3.7			
M			P = 6.6 GEV/C		
495					
525	19.7 ± 23.2			4.4 ± 8.8	
555	36.3 ± 12.5	10.9 ± 18.6	4.8 ± 8.9	7.4 ± 8.3	6.6 ± 6.4
585	56.5 ± 10.3	28.9 ± 10.5	27.0 ± 9.1	7.8 ± 6.2	-1.1 ± 3.9
615	54.8 ± 9.5	37.6 ± 12.1	11.2 ± 7.7	11.3 ± 9.2	5.4 ± 3.4
645	61.1 ± 6.7	36.8 ± 7.4	15.1 ± 8.1	9.5 ± 4.5	4.7 ± 4.3
675	90.4 ± 5.3	49.2 ± 6.6	24.3 ± 5.5	7.6 ± 5.4	1.6 ± 1.8
705	110.2 ± 5.5	70.7 ± 6.6	31.1 ± 4.8	11.3 ± 3.9	6.7 ± 2.6
735	160.8 ± 6.5	77.7 ± 7.2	35.7 ± 5.5	17.8 ± 3.7	-0.2 ± 2.0
765	155.7 ± 7.0	72.3 ± 7.1	30.1 ± 7.2	11.1 ± 4.9	7.1 ± 2.4
795	96.9 ± 5.7	42.5 ± 5.8	20.6 ± 4.7	9.8 ± 5.2	3.9 ± 2.9
825	57.9 ± 4.1	34.1 ± 5.2	14.2 ± 4.4	6.3 ± 2.9	2.5 ± 2.4
855	37.7 ± 4.7	16.3 ± 3.6	8.9 ± 4.9	-0.6 ± 2.6	-1.1 ± 4.8
885	27.9 ± 5.5	8.2 ± 4.5	0.9 ± 2.0	69.2 ± 96.4	1.7 ± 2.4
915	9.2 ± 6.2	6.3 ± 4.2	7.4 ± 4.7		
945	9.2 ± 2.8	6.0 ± 3.1	2.5 ± 5.9		3.0 ± 2.5
975	4.0 ± 2.9				
1005	3.1 ± 3.8	5.9 ± 6.0			

Table 2 (continued)

TABLE 2 CONTINUED

LEAD $\frac{1}{A}\frac{d^2\sigma}{d\Omega dm}$ in $\mu b/sr.MeV/c^2$ vs. $m(MeV/c^2)$, p(GeV/c) and $t_\perp$ $(GeV/c)^2$

-T =	0.001	0.003	0.005	0.007	0.009
M			P = 5.8 GEV/C		
495	33.4 ± 4.9	7.0 ± 7.1	6.2 ± 5.1	0.7 ± 4.5	1.7 ± 2.5
525	30.5 ± 4.2	7.6 ± 5.7	10.3 ± 4.5	2.8 ± 3.1	0.5 ± 0.5
555	35.7 ± 4.8	24.1 ± 5.1	8.8 ± 4.7	3.6 ± 2.9	2.9 ± 2.0
585	37.7 ± 4.6	16.5 ± 5.2	11.3 ± 6.1	1.4 ± 4.4	0.9 ± 0.9
615	42.3 ± 3.3	19.2 ± 4.3	12.2 ± 4.4	2.0 ± 3.3	0.4 ± 1.8
645	46.4 ± 3.6	23.4 ± 4.0	9.0 ± 2.5	-0.1 ± 4.0	1.1 ± 1.3
675	64.0 ± 3.7	35.6 ± 4.9	17.0 ± 3.6	4.0 ± 2.8	4.3 ± 2.7
705	79.9 ± 4.1	40.3 ± 5.3	13.5 ± 4.1	14.4 ± 4.1	2.9 ± 3.8
735	106.5 ± 4.5	57.0 ± 4.9	29.3 ± 5.1	13.4 ± 3.2	4.1 ± 2.3
765	106.1 ± 5.4	43.4 ± 6.0	16.3 ± 5.3	10.5 ± 4.5	6.2 ± 2.9
795	69.9 ± 5.3	25.6 ± 6.3	7.7 ± 4.9	13.5 ± 9.2	15.0 ± 11.4
825	40.6 ± 4.9	16.2 ± 5.5	10.0 ± 3.9	4.9 ± 2.6	2.1 ± 1.6
855	25.0 ± 4.2	16.9 ± 5.8	5.6 ± 2.8	3.9 ± 3.2	
885	12.2 ± 4.4	6.5 ± 3.1	2.2 ± 2.5	7.1 ± 7.2	
915	6.1 ± 3.7		4.2 ± 4.7	6.8 ± 9.6	4.4 ± 6.3
945	2.6 ± 4.5	4.7 ± 3.4	3.4 ± 3.5		
975	11.7 ± 4.5	0.1 ± 7.1		-6.1 ± 12.3	
1005	3.7 ± 3.9				
M			P = 6.2 GEV/C		
495	29.5 ± 10.1	-7.9 ± 22.4	141.1 ± 168.4	-23.9 ± 95.9	
525	40.2 ± 6.7	5.0 ± 6.2	12.4 ± 6.9	3.1 ± 3.5	2.8 ± 2.0
555	33.1 ± 4.9	20.5 ± 6.4	12.7 ± 5.1	4.0 ± 2.3	-1.8 ± 4.1
585	46.2 ± 5.3	25.7 ± 6.5	13.2 ± 6.4	2.6 ± 3.2	0.8 ± 1.6
615	48.5 ± 4.9	15.0 ± 5.3	15.8 ± 4.3	10.8 ± 4.2	0.6 ± 1.6
645	65.8 ± 3.8	26.4 ± 4.7	9.5 ± 3.7	0.2 ± 2.5	1.2 ± 1.1
675	83.6 ± 3.7	38.4 ± 4.5	16.6 ± 3.4	10.0 ± 3.0	4.3 ± 1.2
705	99.0 ± 4.4	47.4 ± 5.0	28.6 ± 4.5	10.7 ± 3.2	2.4 ± 2.3
735	137.6 ± 6.2	61.0 ± 5.3	27.5 ± 5.0	13.2 ± 3.7	1.2 ± 2.3
765	137.4 ± 5.3	65.3 ± 5.8	20.2 ± 5.0	10.0 ± 3.1	2.4 ± 2.0
795	88.3 ± 4.7	39.7 ± 4.7	20.5 ± 4.3	7.1 ± 3.7	2.7 ± 1.8
825	54.9 ± 4.2	20.0 ± 7.8	1.6 ± 3.6	5.8 ± 2.0	4.6 ± 2.5
855	30.8 ± 4.8	11.9 ± 4.7	14.1 ± 4.1	6.1 ± 3.4	-0.0 ± 2.6
885	15.9 ± 4.0	6.2 ± 7.7	3.9 ± 3.2	3.5 ± 2.1	3.1 ± 2.7
915	10.0 ± 2.7	6.0 ± 3.5		0.8 ± 1.6	
945	3.6 ± 4.9	2.3 ± 2.4			
975	4.4 ± 3.2	3.0 ± 3.3		2.4 ± 2.4	
1005	2.7 ± 1.9	0.1 ± 6.6			
M			P = 6.6 GEV/C		
495					
525	38.7 ± 20.4	14.6 ± 15.7	8.2 ± 10.6	14.8 ± 23.1	
555	28.0 ± 7.2	17.8 ± 11.5	23.9 ± 8.1	14.0 ± 7.0	7.0 ± 4.6
585	45.4 ± 6.3	44.2 ± 8.7	20.4 ± 5.9	1.5 ± 3.6	-0.6 ± 2.0
615	56.4 ± 6.8	13.3 ± 8.5	11.7 ± 5.7	-4.4 ± 7.0	4.4 ± 3.1
645	59.5 ± 5.7	37.7 ± 6.6	5.7 ± 4.5	2.9 ± 2.9	1.6 ± 2.6
675	88.3 ± 4.8	49.1 ± 5.9	18.0 ± 4.4	9.8 ± 5.0	5.0 ± 2.1
705	121.2 ± 5.2	67.1 ± 6.3	28.7 ± 4.1	6.6 ± 3.2	2.7 ± 1.9
735	148.6 ± 5.8	73.5 ± 6.6	36.0 ± 5.0	11.8 ± 3.0	2.4 ± 1.7
765	152.7 ± 6.2	72.1 ± 6.3	20.7 ± 5.9	10.8 ± 4.2	5.0 ± 1.7
795	102.9 ± 5.0	54.5 ± 5.6	18.9 ± 4.0	4.4 ± 4.0	2.4 ± 2.2
825	62.9 ± 3.6	25.7 ± 4.1	14.0 ± 3.6	3.8 ± 2.3	0.7 ± 1.7
855	28.8 ± 3.7	14.8 ± 3.0	2.1 ± 3.5	1.1 ± 3.0	1.0 ± 1.9
885	18.4 ± 3.7	11.7 ± 4.4	-1.9 ± 2.8	-3.5 ± 7.0	3.1 ± 2.7
915	11.2 ± 4.4	5.9 ± 3.4	4.0 ± 3.1	2.8 ± 1.9	2.2 ± 2.7
945	5.7 ± 1.9	2.2 ± 1.8		4.2 ± 6.1	2.5 ± 2.0
975	3.2 ± 2.4	9.3 ± 5.8	3.7 ± 5.4		-6.0 ± 12.0
1005	9.5 ± 5.8	4.4 ± 4.5			

Table 2 (continued)

TABLE 2 CONTINUED

URANIUM $\frac{1}{A}\frac{d^2\sigma}{d\Omega dm}$ in μb/sr.MeV/c^2 vs. m(MeV/c^2),p(GeV/c) and $t_\perp$ (GeV/c)^2

-T =	0.001	0.003	0.005	0.007	0.009
M			P = 5.8 GEV/C		
495	14.4 ± 5.4	23.5 ± 9.3	3.6 ± 5.6	-3.3 ± 4.7	
525	21.3 ± 4.5	8.2 ± 6.5	12.3 ± 6.5	3.8 ± 2.6	
555	39.7 ± 5.0	14.7 ± 3.9	7.7 ± 3.5	0.6 ± 2.4	1.6 ± 1.2
585	36.0 ± 4.3	16.7 ± 5.7	10.0 ± 5.7	2.1 ± 3.3	1.9 ± 1.1
615	44.3 ± 3.3	18.8 ± 4.2	6.4 ± 3.3	7.1 ± 2.9	1.6 ± 1.6
645	54.1 ± 3.8	22.1 ± 3.7	13.7 ± 2.6	-0.7 ± 3.2	1.0 ± 0.7
675	59.9 ± 3.5	21.2 ± 3.8	15.9 ± 3.0	3.6 ± 2.0	2.5 ± 1.6
705	78.2 ± 3.5	41.1 ± 4.3	14.0 ± 3.6	3.9 ± 2.7	2.5 ± 2.3
735	97.7 ± 3.7	48.3 ± 3.8	24.2 ± 3.8	11.8 ± 2.3	7.0 ± 1.9
765	93.2 ± 4.3	43.5 ± 4.9	22.6 ± 4.5	9.6 ± 3.4	6.6 ± 2.4
795	68.8 ± 4.6	24.9 ± 5.3	8.9 ± 3.9	11.8 ± 5.1	5.1 ± 9.5
825	41.8 ± 4.8	15.2 ± 6.0	13.3 ± 4.1	9.4 ± 3.3	3.1 ± 2.0
855	18.3 ± 4.0	8.1 ± 3.4	6.3 ± 2.8	7.1 ± 3.4	3.4 ± 2.5
885	7.8 ± 4.6	6.3 ± 3.5	1.1 ± 2.2	0.9 ± 1.7	
915	3.6 ± 3.6	1.1 ± 2.1			
945	2.9 ± 2.9	2.2 ± 3.1	1.4 ± 2.9	1.3 ± 2.6	
975	2.6 ± 3.1	2.8 ± 3.9	1.8 ± 3.6		
1005					
M			P = 6.2 GEV/C		
495	16.4 ± 12.5	22.3 ± 16.7			
525	42.2 ± 8.2	18.9 ± 11.0	4.0 ± 6.6		0.8 ± 1.1
555	34.9 ± 5.6	16.8 ± 7.0	4.6 ± 4.5	5.4 ± 3.0	-1.1 ± 2.9
585	40.7 ± 6.0	26.5 ± 5.7	5.5 ± 5.3	6.3 ± 3.7	1.3 ± 0.9
615	46.1 ± 4.7	21.9 ± 4.8	19.3 ± 4.7	4.7 ± 2.5	-0.2 ± 0.7
645	66.0 ± 3.7	20.4 ± 4.2	12.2 ± 3.6	3.8 ± 2.2	0.7 ± 0.6
675	78.0 ± 3.5	33.9 ± 4.0	11.8 ± 2.7	4.9 ± 2.2	1.8 ± 0.6
705	103.6 ± 4.2	44.3 ± 4.4	22.5 ± 3.9	4.4 ± 2.1	2.5 ± 1.6
735	125.2 ± 5.0	54.1 ± 4.5	24.0 ± 4.2	7.8 ± 2.7	0.4 ± 1.2
765	129.8 ± 4.4	60.4 ± 4.7	23.3 ± 4.4	9.2 ± 2.2	3.9 ± 1.7
795	83.9 ± 4.7	32.6 ± 3.7	18.5 ± 3.2	2.3 ± 2.4	3.0 ± 1.3
825	47.4 ± 3.3	18.6 ± 7.7	9.7 ± 3.3	7.3 ± 1.8	4.3 ± 2.0
855	31.8 ± 4.7	7.3 ± 5.0	7.7 ± 2.8	10.0 ± 3.8	-0.6 ± 3.2
885	21.8 ± 4.6	10.6 ± 10.1	2.5 ± 2.5	0.4 ± 0.8	1.3 ± 1.7
915	6.1 ± 2.0	1.6 ± 1.9	4.2 ± 3.4	1.6 ± 1.9	1.5 ± 2.9
945	1.9 ± 6.3	3.8 ± 4.3	1.9 ± 3.7		
975	3.3 ± 4.8		0.1 ± 5.4	1.1 ± 2.2	
1005	1.2 ± 1.8	2.6 ± 3.7			
M			P = 6.6 GEV/C		
495					
525	56.7 ± 33.4	53.1 ± 40.0	28.4 ± 26.1		
555	34.0 ± 9.8	29.3 ± 16.5	20.6 ± 10.0	4.5 ± 5.1	4.2 ± 4.1
585	40.7 ± 7.5	30.2 ± 8.8	4.1 ± 4.1	7.6 ± 4.2	1.9 ± 2.3
615	41.7 ± 7.2	15.3 ± 7.7	12.7 ± 5.7	6.3 ± 5.3	1.8 ± 1.2
645	68.0 ± 5.9	31.2 ± 5.8	5.1 ± 5.5	5.5 ± 3.0	1.3 ± 1.5
675	82.0 ± 4.6	37.7 ± 5.2	18.4 ± 4.1	5.4 ± 3.5	1.5 ± 1.1
705	117.3 ± 5.0	57.5 ± 5.3	18.1 ± 3.3	7.8 ± 2.5	1.0 ± 0.9
735	150.0 ± 5.6	70.8 ± 6.0	31.1 ± 4.4	8.9 ± 2.3	1.1 ± 1.0
765	150.5 ± 5.8	70.6 ± 5.6	22.7 ± 5.3	6.7 ± 3.0	3.0 ± 0.9
795	99.6 ± 4.4	43.9 ± 4.5	14.2 ± 3.1	4.8 ± 3.0	1.9 ± 1.6
825	61.9 ± 3.0	22.1 ± 3.2	7.3 ± 2.6	2.2 ± 1.6	0.8 ± 1.4
855	29.5 ± 3.2	16.3 ± 2.5	7.7 ± 3.2	-0.3 ± 1.6	0.7 ± 1.5
885	15.8 ± 3.4	7.2 ± 3.6	7.4 ± 3.3	2.3 ± 3.0	0.5 ± 1.1
915	15.8 ± 5.3	8.5 ± 4.5	3.3 ± 2.6	1.0 ± 1.2	0.9 ± 1.8
945	5.4 ± 1.8	5.0 ± 2.7	0.4 ± 3.3	0.9 ± 1.9	
975	5.1 ± 3.2	3.2 ± 4.0	0.8 ± 1.6	3.8 ± 7.7	
1005	1.4 ± 2.7	2.0 ± 4.0			

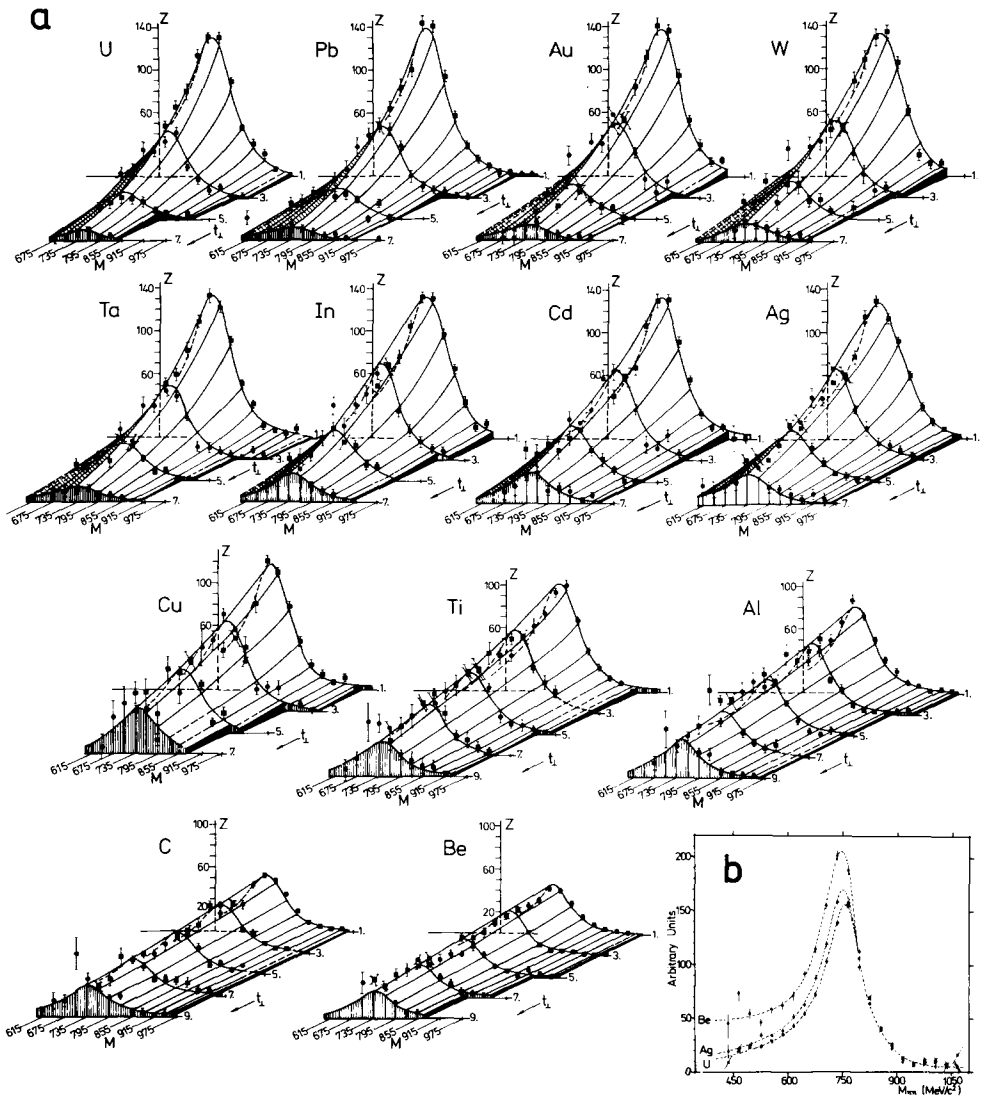

Fig. 3. (a) The cross section $Z = d\sigma/d\Omega dm(\mu b/sr \cdot MeV/c^2 \cdot nucleon)$ as a function of m (MeV/c^2) and $t_\perp$ in units of -0.001 GeV$^2/c^2$ for $p = 6.2 \pm 0.2$ GeV/c. The curves are the best fits to eq. (8) with $R_1(m)$. The background is not drawn. This figure shows about 2% of the data. (b) Mass spectra after removal of production mechanism. (Note that in the absence of background, all spectra would be identical.)

4. ANALYSIS AND RESULTS

The analysis of reaction (1) in terms of ρ-production is complicated because there is no unique theory for wide resonances and the form of the background is not known. It is for these reasons that we have presented the experimental data in table 1 and table 2 free from theoretical assumptions.

4.1. *Analysis of hydrogen data*

To analyze the hydrogen data we have fit the cross sections in table 1 with the following equations

$$\frac{d\sigma}{d\Omega dm} = Cg(p)2mR_1(m) + BG(m,p) , \tag{2}$$

$$\frac{d\sigma}{d\Omega dm} = Cg(p)2mR_2(m) + BG(p,m) , \tag{3}$$

$$\frac{d\sigma}{d\Omega dm} = Cg(p)2mR_3(m) + BG(p,m) , \tag{4}$$

with

$$R_1(m) = r(m)\left(\frac{m_\rho}{m}\right)^4 , \qquad R_2(m) = r(m) + I(m) ,$$

$$R_3(m) = r(m)\left(\frac{m_\rho}{m}\right)^4 + I(m) ,$$

$$r(m, \Gamma_\rho(m)) = r(m) = \frac{1}{\pi}\frac{m_\rho \Gamma_\rho(m)}{(m_\rho^2 - m^2)^2 + m_\rho^2 \Gamma_\rho^2(m)} ,$$

$$\Gamma_\rho(m) = \frac{m_\rho}{m}\left[\frac{(m/2)^2 - m_\pi^2}{(m_\rho/2)^2 - m_\pi^2}\right]^{\frac{3}{2}} \Gamma_0 , \qquad g(p) = p^2\left(1 + \frac{M}{p}\right)^2 ,$$

$$I(m) = \frac{D}{2m}\frac{m^2 - m_\rho^2}{(m_\rho^2 - m^2)^2 + m_\rho^2 \Gamma_\rho^2(m)} ,$$

$$BG(p,m) = \left(\sum_{i=1}^{4} a_i p^{i-1}\right)\left(\sum_{j=1}^{4} b_j m^{j-1}\right) \geq 0 ,$$

where $g(p)$ is the energy dependence of the forward production cross section. If $g(p) = p^2$ ($M = 0$) we have classical diffraction scattering with a con-

stant total cross section. When $g(p) = p^2\,(1 + M/p)^2$ and $M > 0$, then $d\sigma/dt(t = 0)$ decreases with increasing ρ energy. The background function $BG(m, p)$ is the product of two general third-order polynomials in m and p. *The function $I(m)$ is an empirical interference like term different from the one suggested by Soeding* [9]. The terms $r(m)$ and $\Gamma_\rho(m)$ are the relativistic p-wave resonance formulae proposed by Jackson [10].

Eq. (2) represents the fitting of the dipion spectrum to a ρ-production term where the resonance formula is modified by a phenomenological "Ross-Stodolsky" term [11] $(m_\rho / m)^4$ plus a general background. The factor $(m_\rho / m)^4$ also appears in a model by Kramer and Uretsky [11] and has been used at DESY and SLAC [1] to account for the shift and shape distortion of the photoproduced ρ-spectrum. Eq. (3) represents another commonly accepted procedure to fit the spectrum with the mass shift and shape distortion accounted for by an empirical term $I(m)$ whose magnitude D is determined by the fit. Eq. (4) assumes both mechanisms can be present.

Fitting was done in two ways. Firstly, each of functions (2), (3) and (4) was fit to the data of table 1 using the CERN fitting program MINUIT [12]. The following quantities were free parameters in the fits: $a_i, b_j, C, m_\rho, \Gamma_0$, M and D. A lower cut-off limit m_0, used in fitting the data was chosen in the following way: fig. 4a shows two mass spectra from 460 to 1000 MeV c^2. One was taken with a peak bremsstrahlung energy at 7.4 GeV and the other at 7.0 GeV. Both had a central spectrometer momentum of 6.0 GeV c. Since the two spectra are in agreement above 610 MeV c^2 one concludes that the inelastic contribution above this mass is small. The same result was found for spectra at $k_{max} = 5.55$ GeV and 5.25 GeV. Therefore, m_0 was chosen to be 610 MeV c^2. Checks were made by varying $610 < m_0 < 760$ MeV/c^2 and the values of $m_\rho, \Gamma_0, C, M, D$ and the background were found to be insensitive to these changes. Studies were also made on the background function $BG(m, p)$ and it was found that the results of a product of second-order polynomials were consistent with those of the higher order function described above. The values of m_ρ and Γ_0 obtained from all fits done in this manner were consistent with $m_\rho = 765 \pm 10$ MeV/c^2 and $\Gamma_0 = 145 \pm 10$ MeV/c^2.

Secondly, using the values $m_\rho = 765$ MeV/c^2 and $\Gamma_0 = 145$ MeV c^2 obtained above, the mass spectrum for each momentum was fit separately to functions (2), (3) and (4). In this way the cross sections and the background were left with an arbitrary momentum dependence in contrast to the first method where both the cross section and the background were required to be smooth functions of the momentum. The cross sections obtained from these fits were found to be insensitive within the limits of $m_\rho = 765 \pm 10$ MeV/c^2 and $\Gamma_0 = 145 \pm 10$ MeV/c^2 quoted above. Fig. 4b shows the values of $d\sigma/dt(t = 0)$ obtained in this way and they are seen to be insensitive to assumptions (2), (3) or (4). Fig. 4b also includes the results of other experiments where the background has been treated. As seen, these data are in good agreement with the present experiment.

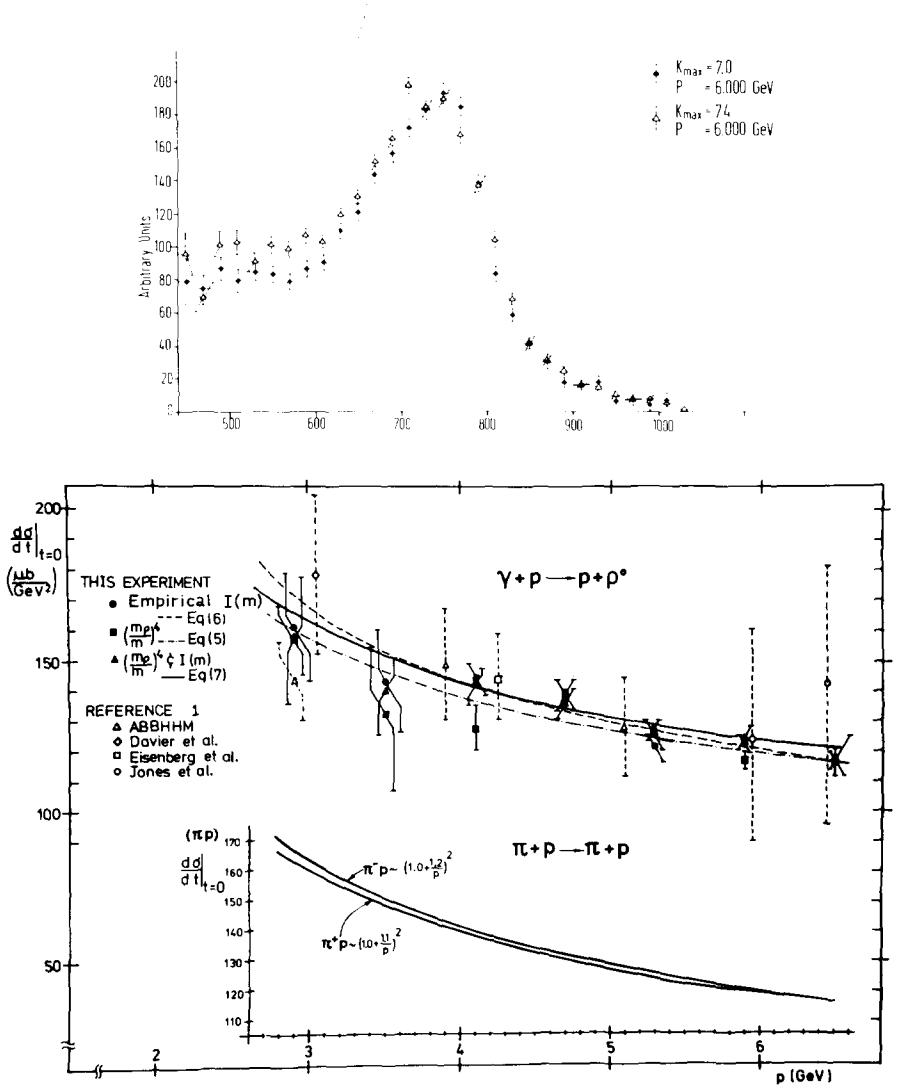

Fig. 4. (a) Comparison of mass spectra for hydrogen for different peak bremsstrahlung energy with the same central spectrometer momentum. The agreement of the spectra above 610 MeV/c^2 indicates the inelastic contribution to the spectra above this mass is small. (b) Comparison to other experiments and results of our measurements on hydrogen obtained by fitting the data matrix (table 1) with eq. (2), (3) and (4). In obtaining $d\sigma/dt$ ($t = 0$) from $d\sigma/d\Omega dm$ the normalization uncertainty of $\pm 10\%$ due to the mass spectrum functions used, is not shown. Also shown is a comparison of the best fits to our cross sections as a function of p, and the πN cross section as a function of p normalized to the same scale.

4.2. *Conclusions from the hydrogen data*

(i) The cross sections $d\sigma/dt(t=0)$ obtained from the fits to expressions (2), (3) and (4) exhibit the following characteristics:

(a) The values for $d\sigma/dt(t=0)$ obtained by fitting eq. (2) (Ross-Stodolsky factor) show a behaviour

$$\left.\frac{d\sigma}{dt}\right|_{t=0} \propto \left(1+\frac{1.0\pm0.3}{p}\right)^2 . \tag{5}$$

(b) When eq. (3) (empirical) is used in the fit, we observe

$$\left.\frac{d\sigma}{dt}\right|_{t=0} \propto \left(1+\frac{1.3\pm0.3}{p}\right)^2 . \tag{6}$$

(c) For fits using eq. (4) (both Ross-Stodolsky and empirical) the observed dependence is

$$\left.\frac{d\sigma}{dt}\right|_{t=0} \propto \left(1+\frac{1.0\pm0.4}{p}\right)^2 . \tag{7}$$

This is to be compared to the momentum dependence of π^+p and π^-p cross sections in the energy region from 3.0 to 7.0 GeV [8].

$$\left.\frac{d\sigma}{dt}\right|_{t=0} \propto \sigma^2_{\pi^+ p}\,(1+\beta_+^2) \propto \left(1+\frac{1.1\pm0.1}{p}\right)^2 ,$$

$$\left.\frac{d\sigma}{dt}\right|_{t=0} \propto \sigma^2_{\pi^- p}\,(1+\beta_-^2) \propto \left(1+\frac{1.2\pm0.1}{p}\right)^2 ,$$

where p is in GeV/c and $\beta_\pm$ = real part/imaginary part for $\pi^\pm$p scattering. Therefore, independent of our assumptions, the energy behaviour of ρ-production is found to be very similar to πN scattering in the same energy region.

(ii) The mass of the rho measured from $\rho \to \pi^+\pi^-$ is about the same as measured by $\rho \rightleftharpoons e^+e^-$, but the width of the rho is about 30 MeV/c^2 higher [13].

4.3. *Analysis of complex nuclei data*

Following the conclusions drawn drom fig. 3, that the dipion spectra are dominated by ρ-production and that the background cannot be neglected, the complex nuclei data were analyzed in the following manner.

The four-dimensional data matrix $d\sigma/d\Omega dm(A, m, p, t_\perp)$ was fit by a theoretical function of the form

$$\frac{d\sigma}{d\Omega dm}(A, m, p, t_\perp) = \frac{1}{\pi}\, p^2 2mR_\rho(m)\,(f_c + f_{inc}) + BG(A, m, p, t_\perp) . \tag{8}$$

The first term represents the main contribution from ρ-photoproduction and the second term the contribution due to a non-resonant background.

$$f_C = f_C(A, t_\perp, t_\parallel, \sigma, \beta) = \left(\frac{\sigma'}{\sigma}\right)^2 \left| 2\pi f_0 \int_0^\infty b\,db \int_{-\infty}^{\infty} dz\, J_0(b\sqrt{|t_\perp|}) \right.$$

$$\left. \times \exp(iz\sqrt{|t_\parallel|})\, \rho(z,b) \exp\left[-\tfrac{1}{2}\sigma'(1 - i\beta) \int_z^\infty \rho(z',b)\,dz' \right] \right|^2 ,$$

$$\sigma' = \sigma(1 - \eta\xi\sigma) , \qquad \xi = \frac{1}{16\pi a} \int \exp(-b^2/4a)\, g(z,b)\, d^2b\, dz ,$$

$$\eta = \eta(\sigma) = \int \exp(-\tfrac{1}{2}\sigma T(b))\, Q(b)\, d^2b \Big/ \int \exp(-\tfrac{1}{2}\sigma T(b))\, T(b)\, d^2b ,$$

$$Q(b) = \int_{-\infty}^{\infty} \rho^2(z,b)\,dz , \qquad T(b) = \int_{-\infty}^{\infty} \rho(z,b)\,dz ,$$

$$\sigma = \sigma_{\rho N} , \qquad a = 8(\mathrm{GeV}/c)^{-2} .$$

Here f_C is the forward-coherent-production cross section [14] where the ρ-meson produced with an effective forward-production cross section $|f_0|^2$ on a single nucleon is attenuated by $\exp(-\frac{1}{2}\sigma' \int_z^\infty \rho\,dz)$ in nuclear matter as it leaves the nucleus. (Gottfried has shown that corrections arising from ρ instability within the nucleus are negligible [15].) The factor $\rho(z,b) J_0(b\sqrt{|t_\perp|})$ comes from the nuclear shape and the term $\rho = \rho_0 \,(1 + \exp[(r - R)/s])$ is the Woods-Saxon density, where R is the nuclear radius and $s = 0.545$ fm. The difference in initial and final mass produces a term $\exp(iz\sqrt{|t_\parallel|})$ and σ' is the effective ρ-nucleon total cross section where we have taken into account second-order correlation effects between nucleons inside the nucleus.

We used the model of von Bochmann et al. [16] to account for the correlation length ξ and the correlation wave function $g(b,z)$. The inclusion of correlation causes a 4% correction to our final results. The ratio of the real part to the imaginary part of the scattering amplitude on a single nucleon, β, was taken to be -0.2, following the analysis of γp cross section measurements [17] at 6.0 GeV. This value is consistent with our preliminary results obtained from interference between $\rho \to e^+e^-$ and Bethe-Heitler pairs [17]. The incoherent production cross section f_{inc} describes the case where the recoil nucleus is left in an excited or fragmented state [18]. The incoherent contribution is largest for low A ($\approx 10\%$) and becomes negligible for $A > 100$. The background function $BG(A, m, p, t_\perp)$ is a general polynomial in $(A, m, p, t_\perp)$ space.

To keep the results general, we tried various commonly used forms for the Breit-Wigner and we list five examples: $R_1(m) \ldots R_5(m)$, defining

$R_4(m) = r(m, \Gamma_0)$, $R_5(m) = r(m)$. The function $R_5(m)$ is the relativistic p-wave resonance formula proposed by Jackson [10] and $R_4(m)$ is $R_5(m)$ with a constant width. We have discussed $R_1(m)$, $R_2(m)$ and $R_3(m)$ in the hydrogen analysis above.

Comparison of the data in the four-dimensional measured cross-section matrix with the theoretical function (8) enables us to determine directly the parameters $m_\rho, \Gamma_0, \sigma_{\rho N}, R(A), |f_0|^2, d\sigma_n/dt(A, \theta = 0^o)$.

Again the fitting was done with the CERN program MINUIT. To reduce the contributions from the incoherent term f_{inc} and the background, we selected data in the region $|t_\perp| < |t_c|$, $t_c = -0.01$ (GeV/c)^2, $4.8 < p < 7.2$ GeV/c and $m > m_c$ with $m_c = 600$ MeV/c^2. Thus we restricted the data to the region where most of the π-pairs come from coherent ρ-production. The determination of the various parameters can be visualized simply in the following way:

(i) To determine the background function $BG(A, m, p, t_\perp)$, fits were made with and without a background term of the form

$$BG(A, m, p, t_\perp) = \left(\sum_{i=0}^{l} a_i(A) m^i\right)\left(\sum_{j=0}^{m} b_j(A) p^j\right)\left(\sum_{k=0}^{n} c_k(A) t_\perp^k\right).$$

The goodness of fit improved considerably for $l = 2$, $m = n = 0$ (see fig. 3a). Thereafter no improvement was noticed by increasing l, m or n. The results of the fits were insensitive to changes in m_c (± 100 MeV/c^2) or $|t_c| < 0.01$ (GeV/c)^2. The percentage background is considerable for low A, but decreases with increasing A and m, being small on uranium (see fig. 3b).

(ii) To determine $R(A)$, the nuclear density parameters, the $t_\perp$ dependence of the data was compared with eq. (8). For each element, independent fits were made to the $t_\perp$ dependence of each of the six mass intervals between 690 and 860 MeV/c^2. In this way six independent determinations of the radius were made for each element, thus avoiding the need to simultaneously fit for $R(A)$, m_ρ, Γ_0, and a mass dependent background. The weighted average of the six radii determinations yields a measurement of the radius and they are shown in table 3 and fig. 5.

The radii for light elements (Be and C) are somewhat different from one mass bin to another. The radius measurement for these elements is therefore sensitive to the form of the nuclear density distribution and the form of the background function used. For this reason, a larger error has been assigned.

For heavy nuclei ($A \geq 27$) the radii determined from each individual mass bin are consistent and also in agreement with the value obtained when the radius, m_ρ, Γ_0, and background are all variables. *Therefore the radius determination of heavy nuclei is independent of* m_ρ, Γ_0, Breit-Wigner *mass distribution formula, the normalization and the vector-dominance model.* In addition they are insensitive to s and β. Being determined from neutral mesons they are free from complications of Coulomb interference. The data yield $R(A) = (1.12 \pm 0.02)\, A^{\frac{1}{3}}$ fm which is the most accurate determination of strong-interaction nuclear radii to date [19]. Our radii are to be

Table 3

Summary of measured radii $R(A)$, typical cross sections $\Sigma_n = d\sigma/dt\ (\theta = 0^\circ,\ t_{\min} = -0.002,\ p = 6.54)\ \mu b/((GeV/c)^2$ nucleon), $\chi^2(A)/DF(A)$, $|f_0|^2$, $\sigma_{\rho N}$ and $\gamma_\rho^2/4\pi$. The cross sections do not include an uncertainty of ±10% due to the normalization of the mass distribution $R_n(m)$. The errors include uncertainties in $R(A)$, m_ρ, Γ_0 and BG.

A	R(A) fm	Σ_1	Σ_2	Σ_3	Σ_4	Σ_5
Beryllium	2.35 ± 0.26	627 ± 31	652 ± 50	678 ± 20	628 ± 20	581 ± 59
Carbon	2.50 ± 0.23	772 ± 52	800 ± 50	822 ± 40	767 ± 31	692 ± 101
Aluminium	3.37 ± 0.16	1322 ± 63	1279 ± 51	1348 ± 36	1319 ± 46	1287 ± 87
Titanium	3.94 ± 0.10	1796 ± 78	1706 ± 66	1749 ± 44	1760 ± 102	1622 ± 84
Copper	4.53 ± 0.11	2099 ± 115	2102 ± 68	2179 ± 60	2203 ± 77	2137 ± 196
Silver	5.35 ± 0.09	2591 ± 79	2585 ± 73	2631 ± 61	2725 ± 139	2594 ± 177
Cadmium	5.40 ± 0.14	2636 ± 93	2583 ± 74	2662 ± 60	2801 ± 90	2584 ± 113
Indium	5.56 ± 0.25	2696 ± 90	2634 ± 74	2713 ± 50	2801 ± 157	2651 ± 115
Tantalum	6.50 ± 0.15	2938 ± 154	2900 ± 131	2980 ± 124	3049 ± 139	2903 ± 199
Tungsten	6.30 ± 0.12	2925 ± 140	2877 ± 75	2959 ± 76	3045 ± 112	3035 ± 229
Gold	6.45 ± 0.27	2948 ± 128	2966 ± 147	3017 ± 69	3118 ± 103	3025 ± 111
Lead	6.82 ± 0.20	3112 ± 93	3167 ± 76	3234 ± 59	3368 ± 174	3165 ± 161
Uranium	6.90 ± 0.14	3070 ± 93	3035 ± 58	3144 ± 45	3235 ± 91	3144 ± 114
$\chi^2(A)/DF(A)$	-	~ 1.2	~1.2	~ 1.2	~ 1.5	~ 2.4
m_ρ (MeV/c^2)	-	765 ± 10	773 ± 10	765 ± 10	743 ± 10	742 ± 10
$\|f_0\|^2$ $\mu b/(GeV/c)^2$	-	118 ± 6	120 ± 7.4	125.3 ± 9	112 ± 6	103 ± 10
$\sigma_{\rho N}$ (mb)	-	26.7 ± 2.0	27.7 ± 1.7	27.9 ± 2.4	24.5 ± 1.9	23.5 ± 2.5
$\gamma_\rho^2/4\pi$	-	0.57 ± 0.10	0.59 ± 0.08	0.58 ± 0.11	0.50 ± 0.09	0.50 ± 0.11

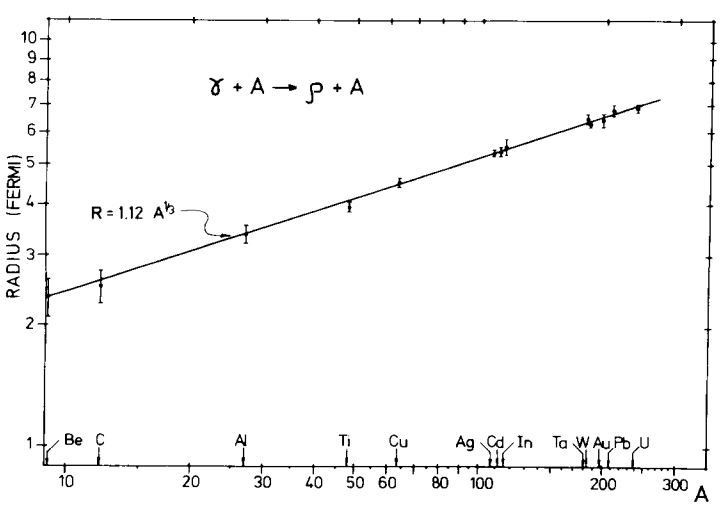

Fig. 5. Nuclear radii obtained from the measured $t_\perp$ dependence of the cross section. Also shown is the best fit to the form $R = R_0 A^{\frac{1}{3}}$.

compared to those determined from electron scattering [20] ($R(A) = 1.08\,A^{\frac{1}{3}}$ fm). A more complete description of our determination of these radii will appear in a later paper.

(iii) To determine m_ρ and Γ_0, the mass and width of the ρ, eq. (8) was compared to the mass dependence of $d\sigma\ d\Omega dm$ for fixed $A, p, l_\perp$. This measured directly the mass and width of the ρ. Independent of the form of the mass distribution used the width $\Gamma_0 = 140 \pm 5$ MeV/c^2. Table 3 shows the fitted results for m_ρ. The mass m_ρ varies from 740 MeV/c^2 to 775 MeV/c^2 depending on the exact forms of $R_n(m)$ used. The best fit values from $R_1, R_2, R_3(m)$ yield $m_\rho = 765 \pm 10$ MeV/c^2.

(iv) To determine the coherent cross section $d\sigma_n/dt(A, \theta = 0^0)$ the data matrix was compared with eq. (8) inserting the measured values of $R(A)$, m_ρ, Γ_0 and BG. Table 3 summarizes some typical cross sections $\Sigma_n = d\sigma/dt(\theta = 0^0, |t_{\min}| = 0.002, p = 6.54)$ μb/(GeV/c)^2 · nucleon, with $k_{\max} = 7.4$ GeV. The index n refers to the mass distribution $R_n(m)$ used to fit the data. The errors in the cross sections include uncertainties in $R(A)$, m_ρ, Γ_0 and BG. Also listed are values for the ratio of chi-squared to degrees of freedom $\chi^2(A)/DF(A)$ for each fit. *Both the "Ross-Stodolsky" form $R_1(m)$ shown in fig. 3a (with $\chi^2(A)/DF(A) \approx 1.2$) and the empirical forms $R_2(m)$ and $R_3(m)$ yield decisively better fits to the data and we choose them as our best results.* Fig. 6 shows the fitted cross sections $d\sigma/d\Omega dm(\theta = 0^0, p = 6.2$ GeV/$c)$ for $R_1(m)$ as a function of m for all elements. The background is also shown and as seen, its contribution (per nucleon) is similar for all elements, indicating that it is incoherent in nature. The ratio of the background to the coherent cross section is considerable for low-A elements but becomes small for high-A elements. Fig. 7 shows the fitted cross sections Σ_1 as a function of A.

(v) To determine $\sigma_{\rho N}$, $|f_0|^2$ and $\gamma_\rho^2/4\pi$ the cross sections were compared with eq. (8) inserting $\beta = -0.2$ and our measured values of $R(A)$. The results corresponding to the various Breit-Wigner forms $R_n(m)$ are listed in table 3. These values are seen to be consistent with each other and we choose representative values based on Σ_1 which are (see fig. 7)

$$\sigma_{\rho N} = 26.7 \pm 2.0 \text{ mb}, \qquad |f_0|^2 = \left.\frac{d\sigma}{dt}\right|_{t=0}(A = 1) = 118 \pm 6\ \mu\text{b}/(\text{GeV}/c)^2$$

and

$$\gamma_\rho^2/4\pi = 0.57 \pm 0.10 .$$

4.4. *Comments on the data and the analysis*

We consider the following to be improvements compared to earlier work [3, 4]:

(i) This experiment has such good statistics that it enables us to make a more detailed measurement of the background, the ρ line shape, the nuclear physics parameters, etc. than was previously possible. (ii) This experiment used twice as many elements. In particular, there are 8 elements with $A > 100$ compared with 1 or 2 elements of previous experiments. The

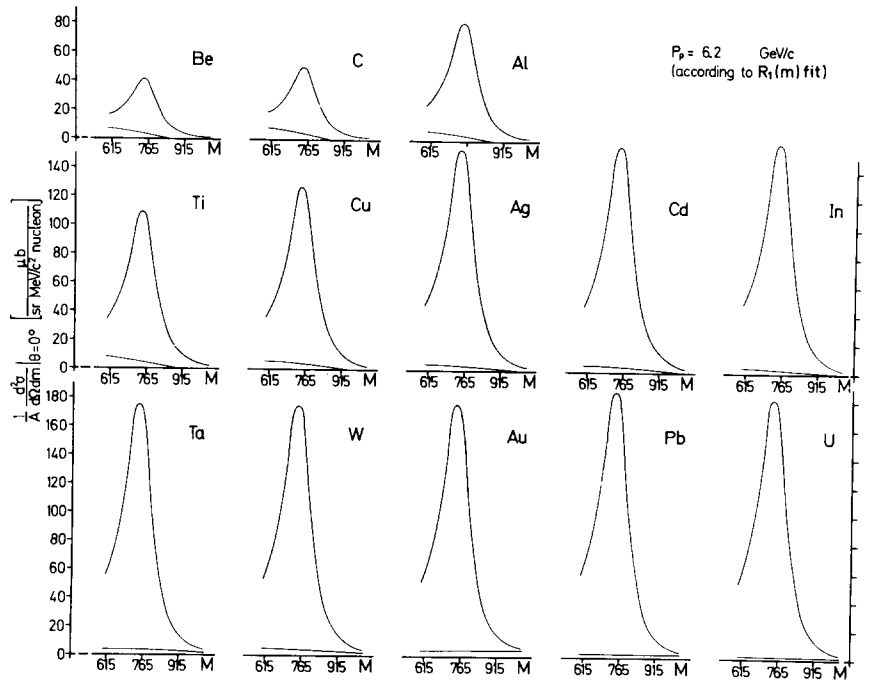

Fig. 6. Fitted cross sections (to $R_1(m)$) $d\sigma/d\Omega dm(\theta = 0^\circ$, $p = 6.2$ GeV/c) and backgrounds as a function of m for all complex nuclei.

large amount of heavy-nuclei data enables us to obtain reliable results with the Margolis model [14] which applies best to heavy nuclei. (iii) The effects of the real part β and nuclear correlations are included in the analysis.

4.5. *Consistency checks*

We present the following examples of checks made to the data (table 2) and analysis:

(i) The directly measured cross sections $d\sigma/d\Omega dm$ agree with the values by Asbury et al. [3].

(ii) To ensure that our results are not sensitive to the nuclear physics of light nuclei, we have analyzed the A dependence by eliminating the data of Be, C, and Al. We also analyzed the data by systematically eliminating each element in turn. The results did not change.

(iii) We have fit various selected subsets of the data with restricted m, p and $t_\perp$ ranges. The results were in good agreement with all values quoted.

(iv) We analyzed the data with a large set of Breit-Wigner mass distributions and the results were consistent with each other (five examples are listed in table 3).

(v) A change in s (= 0.545 fm) of ±10% changes the results by < 2%.

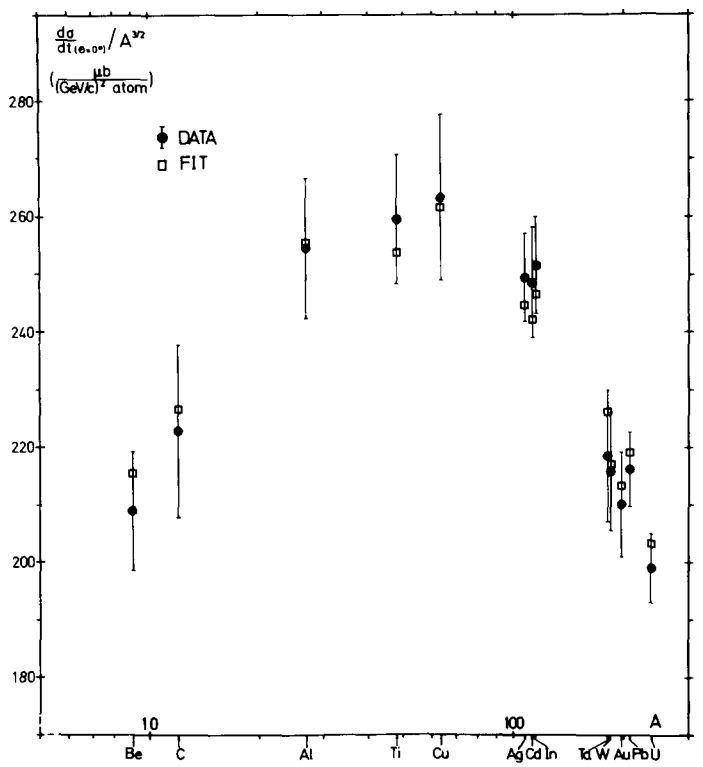

Fig. 7. The values for $\sum_1$ together with the best fit to these results from which we obtain $\gamma_\rho^2/4\pi = 0.57 \pm 0.10$ and $\sigma_{\rho N} = 26.7 \pm 2.0$ mb.

(vi) A change in β of $\pm 50\%$ changes $\gamma_\rho^2/4\pi$ by 10% and changes $R(A)$ by $< 1\%$.

(vii) The measured radii $R(A) = (1.12 \pm 0.02) A^{\frac{1}{3}}$ fm are in agreement with the commonly used values of $R(A) = 1.14 A^{\frac{1}{3}}$ fm (the latter being a $\pm 10\%$ value) [19].

(viii) A change in $R(A)$ by 5% (to $R(A) = 1.18 A^{\frac{1}{3}}$ fm) changes the $\sigma_{\rho N}$ by 1 mb.

(ix) The value $|f_0|^2$ agrees with our measured hydrogen cross section $d\sigma/dt(t=0) = 119 \pm 7\,\mu b/(GeV/c)^2$ at 6.0 GeV/c (fig. 4b).

(x) The value $\gamma_\rho^2/4\pi$ is consistent with the independent determination from measurement of total hadronic cross sections $\sigma_{\gamma A}$ from DESY [21], from the analysis of other vector meson data from complex nuclei by Margolis [22] and with the results of Asbury et al. [3]. (The original value of Asbury et al. was 0.45 ± 0.10. This was obtained using a different nuclear model and did not take into account β and ξ - they are opposite effects - which could produce $\approx 15\%$ effect.)

4.6. *Conclusions of complex nuclei data*

(i) This experiment provides a measurement of the strong interaction nuclear density parameters. (ii) The measured ρ-nucleon cross section agrees with the π-nucleon cross section in the same energy region ($\approx$ 25 mb). (iii) Comparing our values for $\gamma_\rho^2/4\pi$ with the value determined from $\rho \rightleftharpoons e^+e^-$ decay [13] of 0.52 ± 0.07 we conclude that to an accuracy of $\pm 20\%$, the ρ-photon coupling strength does not depend on m_γ, the photon mass, in the range $0 < m_\gamma < m_\rho$. (iv) The results on $\gamma_\rho^2/4\pi$ and $\sigma_{\rho N}$ are in good agreement with the predictions of vector dominance model [5].

We are grateful for the support of Profs. W. Jentschke, V. F. Weisskopf, P. Demos, A. G. Hill and H. Joos, who made this collaboration possible. We wish to thank Drs. S. D. Drell, J. S. Trefil, B. Margolis, A. Dar, R. Wilson, E. Lohrmann, M. Nauenberg, H. Quinn and J. Weber for interesting comments. We are grateful to Drs. H. O. Wuester, D. Lublow, H. Kumpfert, Miss I. Schulz, Miss H. Bock and Mr. P. Berges for technical assistance.

REFERENCES

[1] Cambridge Bubble Chamber Collaboration, Phys. Rev. 146 (1966) 994; 163 (1967) 1510;
J. Ballam et al., Phys. Rev. Letters 21 (1968) 1541; 1544;
L. J. Lanzerotti et al., Phys. Rev. 166 (1968) 1365;
H. Blechschmidt et al., Nuovo Cimento 52A (1967) 1348;
W. G. Jones et al., Phys. Rev. Letters 21 (1969) 586;
ABBHHM collaboration, Phys. Rev. 175 (1968) 1669; Phys. Letters 27B (1968) 54;
Y. Eisenberg et al., Phys. Rev. Letters 22 (1969) 669;
M. Davier et al., Phys. Rev. Letters 21 (1968) 841; Phys. Letters 28B (1969) 619.
[2] G. McClellan, N. Mistry, P. Mostek, H. Ogren, A. Silverman, J. Swartz, R. Talman, K. Gottfried and A. Lebedev, Phys. Rev. Letters 22 (1969) 374.
[3] J. G. Asbury et al., Phys. Rev. Letters 19 (1967) 865; Phys. Rev. Letters 20 (1968) 227.
[4] G. McClellan et al., Phys. Rev. Letters 22 (1969) 377;
J. Swartz and R. Talman, Phys. Rev. Letters 23 (1969) 1078;
F. Bulos et al., Phys. Rev. Letters 22 (1969) 490.
[5] J. J. Sakurai, Lectures in theoretical physics, volume 11 (Gordon and Breach, N. Y. 1968);
H. Joos, Acta Phys. Austriaca, suppl. 4 (1967) 320.
[6] J. G. Asbury et al., Phys. Rev. 161 (1967) 1344.
[7] M. J. Longo and B. J. Moyer, Phys. Rev. 125 (1962) 701.
[8] M. N. Focacci and G. Giacomelli, CERN-report 66-18.
[9] P. Soeding, Phys. Letters 19 (1966) 702.
[10] J. D. Jackson, Nuovo Cimento 34 (1964) 1644.
[11] M. Ross and L. Stodolsky, Phys. Rev. 149 (1966) 1172;
G. Kramer and J. L. Uretsky, Phys. Rev. 181 (1969) 1918.
[12] F. James and M. Ross, CERN 67/623/1.
[13] S. C. C. Ting, Electromagnetics at small distances, leptonic decays of vector mesons and photoproduction of vector mesons, Proc. 14th Int. Conf. on high-energy physics, Vienna, 1968 (CERN, Geneva, 1968) 43.
[14] K. S. Koelbig and B. Margolis, Nucl. Phys. B6 (1968) 85.

[15] K.Gottfried, Bull. Am. Phys. Soc. 13 (1968) 175.
[16] G.v.Bochmann, B.Margolis and L.C.Tang, Phys. Letters 30B (1969) 254.
[17] J.Weber, Ph.D.Thesis, DESY 1969;
H.Alvensleben et al., to be published.
[18] J.S.Trefil, Nucl. Phys. B11 (1969) 330.
[19] J.R.Glauber and G.Matthiae, ISS 67/16:
R.Wilson, Nuovo Cimento Letters 1 (1969) 952.
[20] R.Hofstadter, Ann. Rev. Nucl. Sci. 7 (1957) 231.
[21] H.Meyer, private communication:
E.Lohrmann,DESY 69/21.
[22] G.v.Bochmann and B.Margolis, Phys. Rev. Letters 23 (1969) 939.

NOTE ADDED IN PROOF

After the completion of this work we learned of a recent experiment from a SLAC-UCRL-Tufts group (H. H. Bingham et al., SLAC-Pub-727) on $\gamma p \rightarrow \rho p$ with linearly polarized photons. Taking into account the uncertainty of - 10% in our Ross-Stodolsky spectral function normalization, their result at 2.7 GeV for $d\sigma/dt$ ($t = 0$) from a Ross-Stodolsky fit agrees with our value. At 4.7 GeV, they are about two standard deviations away from ours.

Their fitted results based on the Soeding model, are about 50 - 60 $\mu b/(GeV/c)^2$ smaller than our values obtained from the empirical fits. This most probably comes from the entirely different approaches used in fitting the data. Due to the theoretical difficulties with the Soeding model, such as double counting, gauge invariance, real part of production and omission of other diagrams, etc., we have used a *different* model which is a simple empirical interference-like term plus an important third-order power series in m and p. (See sect. 4 ibid.) The total term is t-independent and does not use any of the pion-nucleon scattering information or any other physical quantities. The term itself is independent of any theoretical assumptions.

In the region $m > 610$ MeV$/c^2$, $t \approx 0$, the 9 fitted coefficients of eq. (3) make it behave like a power series in m and p and yield an effect like the Ross-Stodolsky factor. This approach is completely different from the Soeding model used by the SLAC-UCRL-Tufts group. Their Soeding model, among other things, is t-independent and used the pion-nucleon scattering amplitude calculated from the phase-shift data. Their rho-amplitude is assumed to be helicity conserving in the s-channel c.m. system.